



Physiological and genomic characterization of the
life-cycle stages of the marine coccolithophore
Emiliana huxleyi

Diploma thesis proposed by Sebastian Rokitta

Bremen, December 2008

Acknowledgements

I thank Professor Dieter Wolf-Gladrow and Professor Allan Cembella for administrating and evaluating the work.

Special thanks go to Dr. Björn Rost and Dr. Uwe John! Thanks for boarding me to the PhytoChange project, leading me through the experiments and continuously supervising me throughout the work! Thanks you Björn for your providence in night and daytime! Thank you Uwe for your assistance, reviewing and guidance! I really owe you, guys!

Further I like to thank Dr. Scarlett Trimborn, for the introduction into the laboratory work, for kind supervision especially in the early phase of the project and for critically reviewing earlier versions of this work!

Thanks also are addressed to Klaus-Uwe Richter for maintenance and administration of the MIMS and for his helpful suggestions on any technical questions.

I would also like to thank Ulrike Richter for operating the ANCA as well as Karin Smolla for performing the DIC analysis.

Thanks go also to Sylke Wohlrab, who kindly helped me with the Microarray hybridizations and always was ready to give good input concerning evaluation of the data.

Christoph Völker has really earned thanks for helping me with mathematical as well as programming issues.

Thanks go to Sven Kranz and Nassos Kaffes! I had a really good time with you in lab and office! Thank you, Sven, for critical reviewing the work!

Collective thanks shall be sent to all the members of the BioGeoChemistry group at the AWI for all kinds of stimulating scientific debate, the fun and the really great working atmosphere!

Last, but not least I want to thank my beloved girlfriend Nike. Thank you for all the encouragement. I would not have succeeded without you!

Abstract

Coccolithophore calcification in the open ocean is the main driving force of the marine carbonate pump, significantly contributing to global carbon cycling. Within this group *Emiliana huxleyi* is of special interest due to its global distribution, numerical abundance and the ability to form large blooms. While most work focused on the diploid life-cycle, little is known about the haploid stage, which is unable to calcify. Recent findings indicate that viral termination of blooms induces life-cycle transition and give rise to speculations on the haplonts' ecological role.

To explore the haplonts' ecophysiology, haploid and diploid stages of *E. huxleyi* (TQ 26) were acclimated to photon flux densities of 50 and 300 $\mu\text{mol m}^{-2} \text{s}^{-1}$. The responses in these acclimations were described based on growth rates and elemental as well as isotopic composition. Photosynthetic oxygen evolution as a function of dissolved inorganic carbon and photon flux as well as external carbonic anhydrase (eCA) activities were assessed using membrane-inlet mass spectrometry (MIMS). Short-term ^{14}C disequilibrium incubations were used to estimate the relative contribution of inorganic carbon species to total carbon fixation. Gene expression analysis was performed using microarray approaches.

The diplont showed higher rates of biomass accumulation and photosynthetic oxygen evolution than the haplont. There were significant difference in photosynthetic light use efficiency and light saturation indices. Regarding the modes of carbon acquisition, both life-cycle stages operate a highly-affine carbon concentrating mechanism (CCM) based on direct HCO_3^- uptake. Higher eCA activities and cellular leakage were observed in the haploid stage. In line with the lower photosynthetic activity, microarray analysis suggests a fundamentally different ecological strategy for the haploid stage, resembling the life-style of an ancestral haptophyte. This includes possession of flagella, ability to survive as a mixotroph and potential toxin production.

Introduction

Biological pumps

Phytoplankton is responsible for the vast majority of marine primary production and plays an important role in the global cycling of biogenic elements (Falkowski & Raven, 2007; Schlesinger, 2005). In addition to conventional accumulation of particulate organic carbon (POC) by photosynthesis and subsequent sinking to depth (so-called POC pump), certain key groups of phytoplankton exhibit special functions in biogeochemical cycles: Silicifiers, mainly diatoms, build silicate frustules, which are able to aggregate with organic matter and establish additional and enhanced vertical fluxes of silicon and carbon, respectively. Nitrifying organisms like diazotrophic cyanobacteria fix atmospheric nitrogen (N_2) and thereby provide biologically accessible nitrogen species for the marine ecosystem. Calcifiers, primarily coccolithophores, produce particulate inorganic carbon (PIC) by the precipitation of calcium carbonate ($CaCO_3$), thereby not only removing carbon from the surface ocean, but also sustaining the vertical gradients of alkalinity (Volk & Hoffert, 1985; Rost & Riebesell, 2004). This phenomenon, known as the $CaCO_3$ pump, is an important component of the global carbon cycle, exerts a major influence on climate (Westbroek et al., 1989) and makes calcifiers the object of intensive oceanographic and biogeochemical research.

Both biological pumps are responsible for around 75% of the overall gradient of dissolved inorganic carbon (DIC) between surface oceans and deep sea (Sarmiento et al., 1995). On a global scale, depending on depth, the phytoplankton-driven POC pump conveys about four times more carbon to the deep-sea than the exclusively calcification-driven PIC pump (Broecker & Peng, 1982; Tsunogai & Noriki, 1991). While the POC pump decreases the partial pressure of carbon dioxide (pCO_2) in the surface layer and thus causes oceanic net CO_2 uptake from the atmosphere, the PIC pump has an opposite effect on the air/sea CO_2 exchange and thus can act as a CO_2 source. The relative proportion of both biological pumps, represented by the so-called *rain ratio*, to a large extent determines the net partitioning of CO_2 between ocean and atmosphere. It has to be noted, however, that the efficiency of both pumps may interdepend as PIC may increase the density of aggregates of organic matter and thereby increases the efficiency

of POC export (ballast hypothesis, Armstrong et al., 2002; Klaas & Archer, 2002). In order to understand how a process like photosynthesis and calcification affect seawater chemistry, it is necessary to introduce the marine carbonate system.

Marine carbonate chemistry

The solution of CO₂ in water is, according to Henry's law, directly dependent on the atmospheric pCO₂. Dissolved CO₂ (CO₂ (aq)) reacts with water (H₂O) and forms carbonic acid (H₂CO₃), which has two dissociative levels, bicarbonate (HCO₃⁻) and carbonate (CO₃²⁻, Fig 1). These species together represent the 'dissolved inorganic carbon' (DIC).

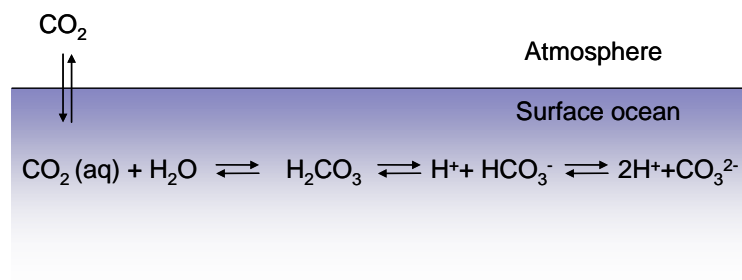


Fig. 1: Schematic illustration of the carbonate chemistry, showing the CO₂ exchange between atmosphere and surface ocean and subsequent reactions to form ionic carbon species and protons.

Although the reactions do not generate net charges, protons (H⁺) are set free, which acidify the seawater and thereby make the carbonate system govern ocean pH conditions. Remarkably, the speciation of DIC and the pH interdepend (Fig. 2), so that speciation is altered when the pH is affected, e.g. by biological activity.

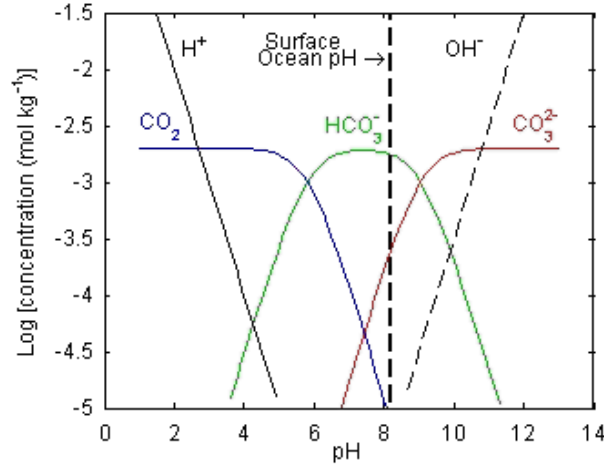
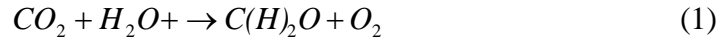
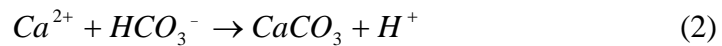


Fig. 2: Equilibrium concentrations of the different carbon species plotted as a function of pH.; Ridgwell & Zeebe, 2005

By photosynthetic organic matter production, [DIC] is decreased in the ambient water:



By precipitating $CaCO_3$ in contrast, calcifying organisms remove charged DIC species from ambient seawater, leaving behind protons:



The decreased pH will in turn force the carbonate system (Fig.2) to re-equilibrate towards higher pCO_2 . Since the protons interact with numerous dissolved buffering anions in seawater, the direct stoichiometrical correlation between pH and the production of calcite is difficult to measure. However, the total excess of proton acceptors over proton donors, i.e. the buffer capacity of the seawater *can* be assessed by a titration (Gran, 1952) and is expressed as total alkalinity (TA; Dickson, 1981):

$$\begin{aligned} \text{Total Alkalinity} = & [HCO_3^-] + 2[CO_3^{2-}] + [B(OH)_4^-] + [OH^-] + [HPO_4^{2-}] + 2[PO_4^{3-}] \\ & [H_3SiO_4^-] + [HS^-] + [NH_3] - [H^+] - [HSO_4^-] - [HF] - H_3PO_4^{3-} \end{aligned} \quad (3)$$

It can be seen that with the precipitation of 1 unit CaCO_3 overall [DIC] is lowered by one unit, but total alkalinity is decreased by 2 units. Because the CO_3^{2-} ion is double-negatively charged, the buffer capacity loses two units of proton acceptors. This way the pH regime is altered, causing a shift to higher pCO_2 . As a result surface water may become oversaturated in CO_2 with respect to atmospheric pCO_2 and thus result in a net release of CO_2 back into the atmosphere (Fig. 3; Zondervan et al., 2001). For this reason, blooms of calcifying algae are, depending on their PIC : POC ratio, smaller sinks for CO_2 than for example diatom blooms.

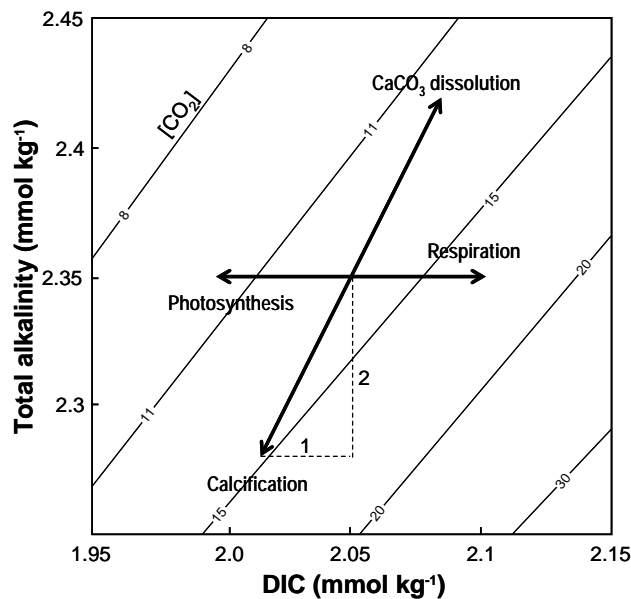


Fig. 3: Changes in the concentrations of DIC, total alkalinity, and CO_2 as a result of calcification; Numbers at the vectors are relative values (modified after Wolf-Gladrow & Zeebe, 2003).

Concerning human induced increase in atmospheric CO_2 and the concomitant ocean acidification (Fig.4), the fate of many marine organisms is at question: Since recent studies (Bijma, 1999; Riebesell et al., 2000; Langdon & Atkinson, 2005) report severe negative impacts on calcification, it is debated whether species diversity of calcifiers is about to decrease significantly. As a further consequence the PIC pump may be constricted to lower efficiency. Zondervan et al. (2001) therefore suggested that decreasing calcification in the future may result in a smaller release of CO_2 to the atmosphere in the future, representing a negative feedback.

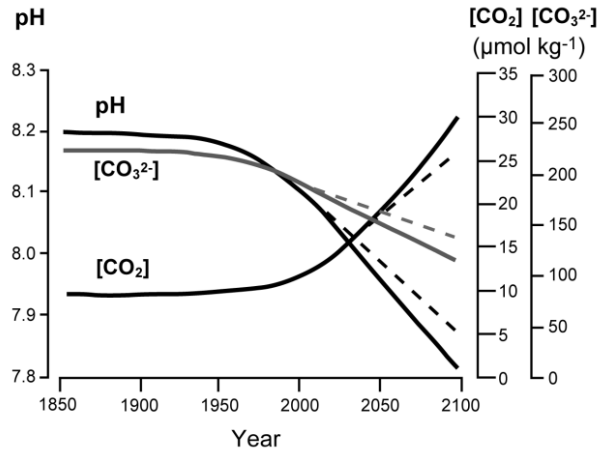


Fig. 4. Seawater pH and the dissolved carbon dioxide (CO_2) and carbonate ion (CO_3^{2-}) concentrations in the surface layer of the ocean assuming a “business as usual” (IS92a, IPCC 2001) anthropogenic CO_2 emission scenario (Houghton et al. 2001). Dashed lines represent the predicted changes in carbonate chemistry if CO_2 emissions are reduced according to the Kyoto Protocol (modified after Wolf-Gladrow et al. 1999).

Coccolithophores

Coccolithophores are considered to be the most productive group of calcifying organisms in the contemporary oceans. This diverse group of marine unicellular phytoplankton modifies chemical conditions within cellular vesicles in such way, that CaCO_3 can precipitate and crystallize along organic structures. Upon exocytosis of this so-called coccolith, it will, together with persisting coccoliths, become part of the coccosphere (Fig. 5).

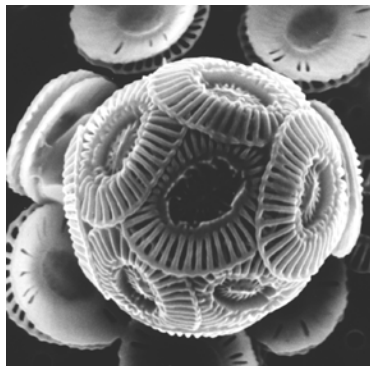


Fig. 5: Coccosphere of *Emiliana huxleyi*, scanning electron micrograph, B.Rost

Many functions for the coccosphere have been proposed, among them control of buoyancy, enhanced light harvesting and grazing protection, but none of those could be proven in labs or observed in field work (Paasche, 2002). Another point under debate is the function of calcification as a carbon concentration mechanism (CCM) for photosynthesis: Many conceptual models have been proposed towards this topic (Paasche, 1964; Sikes, 1980; Anning 1996, McConnaughey, 1998), but since calcification also occurs in the dark (Paasche, 2002) and photosynthesis persists even when calcification is absent or reduced due to low Ca^{2+} availability in the media (Paasche, 2002; Trimborn, 2007), strong evidence for the suggested functional coupling is still lacking.

Especially the species *Emiliana huxleyi* has been in the center of intensive research: It is the most abundant coccolithophore, accounting for 20-50% of the total coccolithophore community in most oceanic areas and up to 100% in subarctic and subantarctic waters (Winter et al., 1994; Balch et al, 1991; Mohan et al., 2008). In comparison with most other coccolithophores its ability to form large blooms, often in context of annual spring succession, is most noticeable: Coccoliths, which are detached when cells run into nutrient depletion/limitation, turn the water milky and can be seen even from outer space. Phytoplankton bloom events are crucial components of ecological succession in marine habitats and periodically provide massive short-term inputs of carbon and/or nitrogen to the ocean food webs. The apparently highly affine uptake of phosphate and the presence of an external alkaline phosphatase make *E.huxleyi* the most competitive under phosphorus (P) limitation (Egge & Heimdal, 1994). It has been shown, that next to grazing, the viral termination of blooms is an important regulatory element of marine ecological succession (Bratbak, 2003). Recent research furthermore indicates, that virus mediated termination of *E.huxleyi* blooms induces life-cycle transition of affected populations (Frada *et al.*, 2008).

Planktonic life-cycle stages

In most sexually reproducing metazoa the life-cycle stages are completely different in form, the diploid (2N) stage being an independent individual forming haploid (1N)

gametes which upon fusion generate a new individual. In phytoplankton, however, haploid and diploid stages of species can exist independently, differently well adapted to their habitats, having more or less similar phenotypes and often being capable of independent vegetative reproduction (Green et al, 1996). Dinoflagellates for example, a large group of marine phytoplankton, are shown to exist primarily in haploid life-cycle stages, which after massive blooming undergo sexual fusion and form diploid cysts, dormant stages that sink to depth and function as seeds for the next bloom event (Anderson et al., 1983). Many diatoms, on the other hand, have been shown to exist primarily in diploid form that propagates by binary fission and over the generations decreases in size due to the reproductive geometry of their silicate frustules. When reaching a certain size-threshold, sexuality is induced, resulting in the formation of haploid spores, which can either become dormant stages or form gametes. Fusion of gametes can then generate new, full-sized individuals (Davidovich & Bates, 1998).

Recent findings of dissimilar coccolithophores belonging to different life-cycle stages of the same species (Billard, 1994; Geisen et al., 2002) accumulate more evidence for a haplo-diploid life-cycle in coccolithophores involving sexual reproduction. Moreover, findings implicate fundamentally different physiologies of ploidy levels, concerning modes of calcification, for example intra- vs. extracellular crystallization of calcite in haploid and diploid stages of the species *Coccolithus spec.* and *Calcidiscus spec.* (Houdan et al. 2004). *E.huxleyi* for instance, has for several decades been known to exist in the diploid, coccolith-bearing form (C-cell) and as a haploid non-calcifying form occurring as scale-bearing swarmers (S-cell, Klaveness, 1972). A third, non-motile naked form that occurs in culture has also been described by Klaveness (1972) that was later shown to be diploid (Green et al. 1996). Since there is no difference in ploidy with respect to the C-cells, and no N-cells have been observed in nature, N-cells are considered to be culture artefacts, mutations of C-cells having lost the ability to calcify (Paasche, 2002).

Given these findings, the results of Frada *et al.* (2008) assign a much greater ecological function than previously assumed to the haploid stage, that's ecophysiology has yet received relatively few attention: Since the haploid, non-calcifying stage is immune to viral attacks, survivors may even benefit from nutrient rich post-bloom-termination

environments and form new inocula for diploid offspring populations in another time and place. Since the haploid phase is not obliged to undergo sexual fusion, haploid populations can persist independently for long times, indicating a rather balanced life-cycle in contrast to those in most diatoms and dinoflagellates. Due to the fact that the haploid life-cycle stage does not calcify, is not susceptible to viral attacks and has a significantly different phenotype, it must be assumed that its metabolic and physiological properties also significantly differ from the diploid stage's. This implicates, that also its ecological potential might differ, for example in mechanisms for the acquisition of inorganic carbon (C_i) for photosynthesis, interspecific competitiveness or modes of trophic biomass acquisition.

Goals of this study

Since life-cycle stages of *E. huxleyi* are obviously severely different they may respond differently to future environmental changes, such as ocean acidification, or decreased stratification and thereby altered light regimes. Owing to their different effect on carbonate chemistry a shift in dominance may provide feedbacks not only to biodiversity, phytoplankton community composition, but also to atmospheric pCO_2 . This study therefore seeks to elucidate metabolic properties and physiological key parameters of the haploid and diploid stages of *E. huxleyi* strain TQ26, by comparing them under different light conditions. Next to determining growth rates, elemental composition analyses were conducted to assess key parameters of biomass accumulation and isotopic fractionation during the acclimations. Comparative physiology by means of *in vivo* bioassays, were performed to examine the light and DIC dependence of photosynthetic oxygen evolution as well as activity of extracellular carbonic anhydrases (CA) of acclimated cultures. Isotopic labeling techniques were used to examine and quantify C_i -uptake preferences during photosynthesis. Gene expression analyses were conducted to assess transcriptomic responses on life-cycle transition and light intensity to characterize genes or metabolic pathways being exclusively regulated as an effect of ploidy level and light acclimations.

Materials and Methods

Acclimation

Culture conditions - Haploid and diploid cells of the *E. huxleyi* strain TQ26 (kindly provided by Dr. Ian Probert, Roscoff culture collection) were grown at 15°C in 0.2 µm filtered F/2_R-medium (Guillard and Ryther 1962) enriched with nitrate (NO₃⁻) and phosphate (HPO₄²⁻) according to the Redfield ratio of 16:1 (Redfield, 1963).

Tab. 1: Concentrations of nutrients, trace metals and vitamins added to sea water

Nutrient	Final concentration in F/2_R medium
Na ₂ HPO ₄	6.25 µM
NaNO ₃	100 µM
Na ₂ EDTA	13.4 µM
FeCl ₃	1.8 µM
MnSO ₄	0.915 µM
ZnSO ₄	0.0765 µM
CoSO ₄	0.0425 µM
CuSO ₄	0.0395 µM
Na ₂ MoO ₄	0.0260 µM
Cobalamin	1 µg L ⁻¹
Biotin	1 µg L ⁻¹
Thiamin	200 µg L ⁻¹

Cultures were exposed to light intensities of 50 and 300 µmol photons m⁻² s⁻¹ provided by daylight lamps Biolux 965 (OSRAM, Munich, Germany) under a 16:8h light:dark cycle. Light intensities were adjusted using a datalogger (Li-Cor, Lincoln, USA) with a 4π-sensor (Walz, Effeltrich, Germany). The cells were acclimated to culture conditions for at least two weeks prior to sampling. The 900 mL cylindrical flasks were continuously bubbled with ambient air to avoid cell sedimentation. To ensure that the target seawater carbonate chemistry (~380 µatm CO₂) was unaltered over the course of the experiments

only cultures were used for measurements, in which the pH did not deviate more than 0.05 pH units (NBS scale) from a cell-free reference medium. Cells have been harvested during exponential growth and cell densities never exceeded 120000 cells ml⁻¹ (on average 90000 cells ml⁻¹). The pH was monitored daily using a pH3000 microprocessor pH-meter (WTW, Weilheim, Germany). Samples were taken at least 4 hours after the start of the light period ensuring the cells being photosynthetically highly active. Samples of culture medium (prior to inoculation of cells) and cell-free medium (after harvesting) were taken to determine DIC and TA for detailed description of the carbonate system (Tab.2). DIC was measured colorimetrically according to Stoll et al. (2001) using a TRAACS CS800 autoanalyzer (Seal, Milwaukee, USA). Total alkalinity was inferred from linear Gran-titration plots (Gran, 1952), which were produced using an automated burette system consisting of a Dosimat 665 and pH-Meter 713 (Metrohm, Herisau, Switzerland).

Table 2: Parameters of the carbonate chemistry present in the cultures

	DIC [μmol kg ⁻¹ SW]	TA [μmol kg ⁻¹ SW]	pH (NBS)	pCO ₂ [μatm]
Cell free reference	2235.6 ± 12.3	2462.3 ± 13.5	8.22 ± 0.029	387.5 ± 28.4
1N LL	2219.5 ± 20.2	2444.3 ± 24.6	8.20 ± 0.045	389.0 ± 24.7
1N HL	2204.4 ± 24.8	2430.5 ± 10.2	8.26 ± 0.029	348.1 ± 23.7
2N LL	2131.0 ± 7.0	2317.0 ± 8.7	8.16 ± 0.016	434.6 ± 18.0
2N HL	2121.9 ± 15.7	2321.7 ± 5.3	8.18 ± 0.038	408.7 ± 41.1

Elemental composition - For analysis of total particulate carbon (TPC), particulate organic carbon (POC) and particulate organic nitrogen (PON), cells were filtered onto precombusted (15 h, 500°C) glass fiber filters (1.2 μm; Whatman, Maidstone, UK) by applying a vacuum pressure of below 800 mbar. To determine the POC, i.e. the cells without CaCO₃, respective filters were soaked with 200μL 0.2M hydrochloric acid (HCl) to remove calcite. PIC contents were assessed as the difference in carbon content between

TPC and POC. PON measurements were performed on all TPC and POC filters. Analysis was performed using an ANCA-SL 20-20 mass spectrometer (SerCon Ltd., Crewe, UK). Contents of TPC, POC and PON were normalized to yield cellular quotas.

Isotopic fractionation

The isotope fractionation during POC formation (ϵ_p) was calculated from the isotopic compositions of the carbon source (i.e. CO_2 by definition) and the isotopic composition of the sample (i.e. biomass). For this purpose the isotopic composition of POC was measured (using the same mass spectrometer as for the elemental analysis) and reported relative to the PeeDee belemnite (PDB) standard (Eq.3):

$$\delta^{13}\text{C}_{\text{Sample}} = \left[\frac{(^{13}\text{C}/^{12}\text{C})_{\text{Sample}}}{(^{13}\text{C}/^{12}\text{C})_{\text{PDB}}} - 1 \right] * 1000$$

(3)

The isotopic composition of DIC ($\delta^{13}\text{C}_{\text{DIC}}$) was mass-spectrometrically analyzed in the UCD Stable Isotope Lab of Dr. Howard Spero, Davis, California. From these results, the isotopic composition of CO_2 ($\delta^{13}\text{C}_{\text{CO}_2}$) was calculated after Rau et al. (1996, based on Mook et al. 1974, Eq. 4):

$$\delta^{13}\text{C}_{\text{CO}_2} = \delta^{13}\text{C}_{\text{DIC}} + 23.644 - \left(\frac{9701.5}{T_k} \right) \quad (4)$$

ϵ_p was then calculated following Freeman & Hayes (1992, Eq. 5):

$$\epsilon_p = \frac{\delta^{13}\text{C}_{\text{CO}_2} - \delta^{13}\text{C}_{\text{POC}}}{1 + \frac{\delta^{13}\text{C}_{\text{POC}}}{1000}} \quad (5)$$

Due to the fact, that RubisCO discriminates against the heavier ^{13}C , formed biomass is normally depleted in ^{13}C with respect to the isotopic composition of the carbon source, CO_2 . When HCO_3^- , which is enriched in ^{13}C relative, functions as the primary external source for photosynthetic carbon fixation, the overall ϵ_p is correspondingly decreased. Fractionation can be expressed as a function of the relative proportion of HCO_3^- usage (α), the fractionation constants of RubisCO (ϵ_f , ~28‰, Raven & Johnston, 1991) and the equilibrium fractionation between CO_2 and HCO_3^- (ϵ_s , ~-10‰, Mook et al., 1974), as well as the cellular CO_2 leakage. The latter is expressed as the ratio of cellular CO_2 efflux to gross DIC uptake (Sharkey & Berry, 1985):

$$\epsilon_p = \alpha * \epsilon_s + \epsilon_f * \frac{\text{CO}_2 \text{ efflux}}{\text{Gross DIC uptake}} \quad (6)$$

Since α was known from the ^{14}C disequilibrium method, Eq. 13 could be resolved to obtain the cellular leakage, which represents the ratio of CO_2 efflux to gross DIC uptake (Fig. 28).

Growth rates - Cell densities were assessed on a daily basis in 24 ± 0.5 h intervals using a Multisizer 3 (Beckman-Coulter, Fullerton, USA) and growth rates (μ) were calculated from the increments, i.e. from the difference of final cellcount ($N_{t \text{ final}}$) to initial cellcount ($N_{t \text{ initial}}$) from the measuring interval (t) (Eq. 6).

$$\mu = \frac{\ln(N_{t \text{ final}}) - \ln(N_{t \text{ initial}})}{\Delta t} \quad (6)$$

Further multiplication of POC, PIC and PON contents per cell with μ yielded daily POC, PIC and PON production rates ($\text{pg cell}^{-1} \text{ d}^{-1}$).

Chlorophyll assessment - Results were normalized towards cell counts and/or chlorophyll a (Chl *a*) content of examined cultures. The latter was determined

fluorometrically after extraction in 90% acetone (following JGOFS, 1994) using a TD-700 Fluorometer (Turner Designs, Sunnyvale, USA). The fluorometer was calibrated with standardized solutions of Chl *a* (Sigma, Steinheim, Germany) in 90% acetone (Sigma, Steinheim, Germany).

Bioassays

MIMS assays - Physiological assays on photosynthetic O₂ evolution as well as carbonic anhydrase activity were conducted using membrane-inlet mass spectrometry (MIMS). In this technique algae are incubated in a light- and temperature-controlled cuvette system. The cuvette is separated from an evacuated inlet system by a 0.01 mm thin Teflon® membrane. Dissolved gases in the cuvette can permeate the membrane and are via the inlet system directed to a sector-field mass spectrometer (Isoprime, MicroMass, Manchester, UK). The advantage of using MIMS is the simultaneous real-time measurement of CO₂ and O₂ and their respective isotopes.

Calibration - O₂ and CO₂ signals were calibrated on a daily basis prior to the assays. O₂ signals were inferred from air-equilibrated (21% O₂) buffered assay medium (50mM 4-(2-hydroxyethyl)-1-piperazineethanesulfonic acid (HEPES) F/2_R-medium, pH 8.1). O₂ minimum abundance was measured after the addition of 20 µL saturated sodium dithionite solution, a strong reductant that fully removes free O₂. From the difference in signal heights the molar O₂ concentrations could be assigned using salinity and temperature dependent O₂ solubilities (Weiss, 1970). Ambient argon (Ar) signals were used to correct for deflections in the O₂ signal that do not originate from biological activity. Furthermore the O₂ signal was corrected for the daily machine-inherent O₂-consumption rate (Eq. 8).

$$O_2 \text{ consumption} = \frac{\Delta[O_2]}{\Delta t} = [O_2] * a + b \quad (8)$$

The CO₂ baseline was determined by adding sodium hydroxide (NaOH) to a final effective concentration of 45 mM into the CO₂-free assay medium. Due to the pH of >12, dissolved inorganic carbon will only exist in the form of CO₃²⁻ (Fig.2). Molar CO₂ abundances were calibrated by adding standardized amounts of DIC in form of sodium bicarbonate (NaHCO₃) solution into 0.2M HCl. Since at pH <1 all inorganic carbon will be in the form of CO₂, abundances measured by MIMS can be related to molar concentrations of CO₂ in the cuvette.

By adding known amounts of DIC in form of NaHCO₃ to the buffered assay medium, the pH dependent ratio of [DIC] and [CO₂] can be inferred, allowing calculation of [DIC] from the CO₂ signals during the assay. Since O₂ exerts ionization effects on the CO₂ signal, measured CO₂ signals had to be corrected. By plotting increasing [O₂] versus the influenced [CO₂] in a CO₂-free medium (pH>12), a slope is obtained, representing the influence factor on CO₂. CO₂ signals are then corrected by subtraction of ([O₂] * factor). Acquired calibration data was collected and averaged, the calculated intercalibrative errors can be seen from Tab.3:

Tab. 3: Intercalibrative errors in MIMS assays; 'A' is arbitrary abundance units

	Average	SD [%]
[μM O ₂ /A]	0.00051474	11%
[μM CO ₂ /A]	0.00272462	14%
O ₂ influence factor (A CO ₂ /A O ₂)	0.00017571	15%

To determine the gas exchange of the cells, cultures were concentrated by gentle filtration (1.2 or 3μm polycarbonate filters, Millipore, Billerica, USA) and culture medium was successively exchanged with buffered assay medium. For experiments, 8 ml of cell-suspension were transferred to the MIMS-coupled cuvette and bovine carbonic anhydrase (Enzyme Class 4.2.1.1) has been added to a final effective concentration of 50 μg mL⁻¹. The enzyme drastically accelerates the equilibration between CO₂ and HCO₃⁻, so that changes in total DIC will be immediately reported in the CO₂ signals.

Photosynthesis vs. irradiance - Photosynthetic O₂ evolution was assessed as a function of light intensity. To this end, cells were exposed to light intensities from 25 up to 700 μmol photons m⁻² s⁻¹ during consecutive light-dark periods. Assays were performed under acclimation DIC concentrations of ~2.1 mM (Tab.2). Obtained photosynthesis curves were fitted as a function of photon flux density (PFD; Eq.9). Half-saturation constants (K_{1/2}), maximum photosynthetic rates (V_{max}) and compensation points (K_p) were acquired from the fit curve. The initial light limited slope was measured and the initial angle of the curve was calculated as its arcustangens function. The light saturation index I_k was obtained by interpolating the slope and calculating the intercept with V_{max}. Division of V_{max} by the obtained I_k yielded the respective maximum light use efficiencies α [μmol O₂ (mg Chl a)⁻¹ h⁻¹ * (μmol photons m⁻² s⁻¹)⁻¹].

$$Photosynthesis\ rate_{PFD} = \frac{V_{max} * (PFD - K_p)}{(K_{1/2} + PFD - (2 * K_p))} \quad (9)$$

Photosynthesis vs. DIC/CO₂ - To measure the dependence of photosynthetic O₂ evolution on [DIC], cells were transferred into DIC-free buffered assay medium. In consecutive light-dark periods cells were exposed to the respective acclimation light intensities of 50 and 300 μmol photons m⁻² s⁻¹. Increasing amounts of DIC were added during the dark phases. For the photosynthesis vs. [DIC] plots the dataset was fitted as a function of [DIC] (Eq.10).

$$Photosynthesis\ rate_{[DIC]} = \frac{V_{max} * [DIC]}{K_{1/2} + [DIC]} \quad (10)$$

V_{max} and K_{1/2} were again calculated as the parameters of the fitted curve. Rates of O₂ evolution were also plotted against [CO₂] to obtain half saturation constants for CO₂ concentrations.

CA activities assays - To assess activities of external (eCA) and internal (iCA) carbonic anhydrases, the method of Silverman (1982) was used. In this assay the ^{18}O depletion of doubly-labeled $\text{H}^{13}\text{C}^{18}\text{O}_3^-$ due to hydration and dehydration processes is recorded over time. Concentration changes of the isotopically labeled CO_2 species $^{13}\text{C}^{18}\text{O}_2$ (m/z 49), $^{13}\text{C}^{18}\text{O}^{16}\text{O}$ (m/z 47) and $^{13}\text{C}^{16}\text{O}^{16}\text{O}$ (m/z 45) were followed and the depletion in ^{18}O label was calculated with Eq. 11.

$$\log(^{18}\text{O enrichment}) = \log \frac{(^{13}\text{C}^{18}\text{O}_2) * 100}{^{13}\text{CO}_2} = \log \frac{(m/z 49) * 100}{(m/z 45) + (m/z 47) + (m/z 49)} \quad (11)$$

By comparing the rate of depletion of ^{18}O label, before (S_1) and after (S_2) addition of cells to the assay (Fig. 6), eCA activity can be calculated according to Badger & Price (1989), and were normalized to Chl *a* (Eq. 12):

$$U = \frac{(S_2 - S_1) * 100}{S_1 * \mu\text{g Chl } a} \quad (12)$$

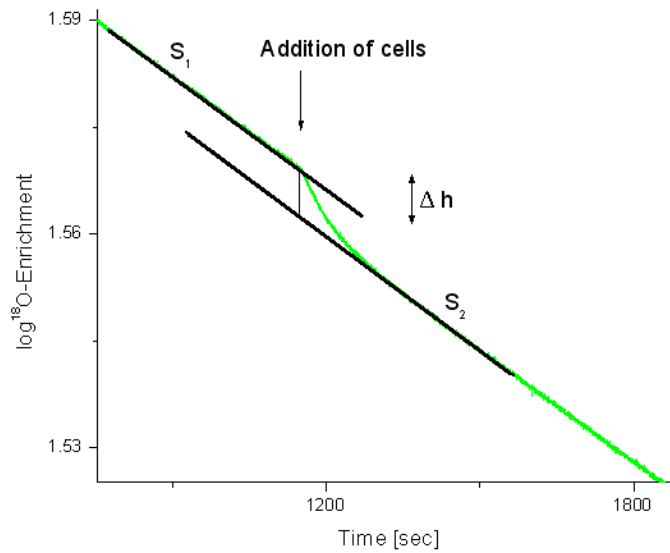


Fig 6: Measurement of eCA and iCA, indicating slopes S_1 , S_2 and Δh

According to Palmqvist et al. (1994), the relative activity of iCA was deduced from the difference in signal heights (Δh) of the extrapolated slope of S_2 and S_1 at the time of cell addition. Obtained activities were normalized to Chl *a*.

¹⁴C disequilibrium techniques - Using the ¹⁴C disequilibrium approach (Espie & Colman, 1986, Elzenga et al. 2000), uptake preferences for CO₂ or HCO₃⁻ were assessed. HCO₃⁻/CO₃²⁻ cannot be discriminated in this approach, both species will therefore be referred to as HCO₃⁻ hereafter. In this technique an illuminated alkaline (pH 8.50) cell-suspension at steady state photosynthesis is spiked with a neutral solution of NaH¹⁴CO₃ (pH 7.0). This way a transient disequilibrium is induced with initially high concentration of ¹⁴CO₂ (~20 % of DIC) that decays exponentially towards equilibrium concentration with time (~0.04 % of DIC; Fig. 7). Phytoplankton that exclusively takes up CO₂ will therefore show high ¹⁴C incorporation rates in the beginning of the assay. Since the concentrations of H¹⁴CO₃⁻ remain fairly constant over the course of the assay (Fig.7A), phytoplankton that takes up HCO₃⁻ will show linear uptake rates (Fig. 7B). As a disequilibrium approach, this technique requires absence of eCA activity, which can be ensured by the application of respective inhibitors.

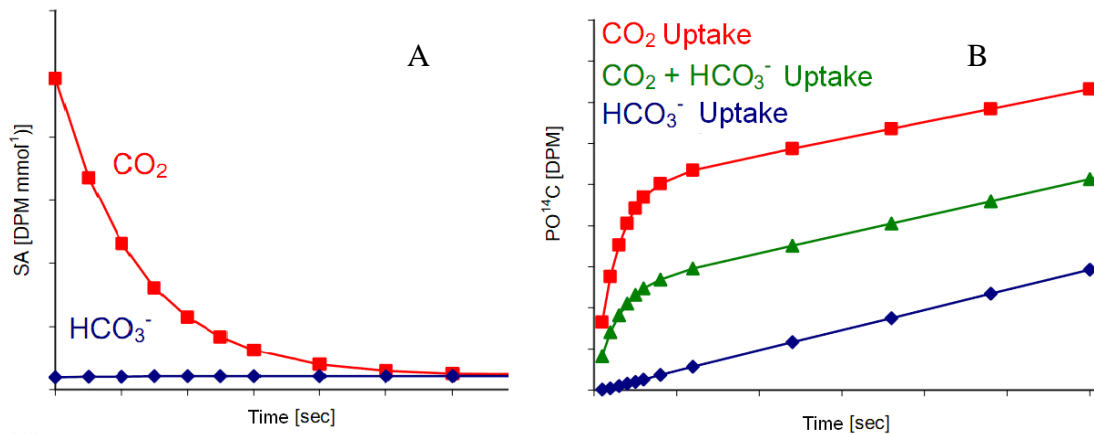


Fig. 7: Theoretical time-course of specific activities of CO₂ and HCO₃⁻ after spiking (A); Theoretical curves of ¹⁴C Fixation in the ¹⁴C disequilibrium approach (B); Note that kinetics are temperature dependent. Graphics: S.Kranz, 2006, modified.

For the ^{14}C disequilibrium experiments cells were concentrated by gentle filtration (polycarbonate filters, 1.2 or 3 μm , Millipore) and culture medium was successively exchanged with assay medium (50mM [N,N-Bis(2-hydroxyethyl)glycine] (BICINE) F/2_R medium, pH 8.5 at 15°C). Radioactive spikes were prepared by adding 10 μL of $\text{NaH}^{14}\text{CO}_3$ solution (GE Healthcare, Piscataway, USA) into 190 μL HEPES-buffered MilliQ Water (pH 7.00), yielding an activity of 740 kBq. Prior to the addition of the ^{14}C spike, 4mL of cell suspension were irradiated with the respective acclimation light intensity for 6 minutes to achieve steady-state photosynthesis. After the addition of the ^{14}C - spike, samples were taken in short time intervals and dispensed into 2mL 6M HCl to stop carbon fixation processes. Non-incorporated $^{14}\text{C}_i$ was removed by degassing over night. After addition of scintillation cocktail (10mL Ultima Gold AB, Packard) samples were measured with a Packard Tri-Carb Liquid scintillation counter (GMI, Ramsey, USA). To correct for residual $^{14}\text{C}_i$ that was not removed, blank measurements were produced using cell-free aliquots of assay medium.

Experiments were run in presence of 50 μM dextrane-bound sulfonamide (DBS, BioCarb, Lund, Sweden), an inhibitor of eCA. Control experiments without DBS were performed to qualitatively assess activity of eCA. Scintillation data was used to infer time-courses of ^{14}C accumulation following Rost et al. (2007, Eq. 13, modified after Elzenga et al., 2000):

$$DPM_t = \frac{V_t(1-f) * (\alpha_1 t + \left(\frac{\Delta SA_{CO_2}}{SA_{DIC}}\right) * (1 - e^{-\alpha_1 t}))}{\alpha_1} + \frac{V_t(f) * (\alpha_2 t + \left(\frac{\Delta SA_{HCO_3^-}}{SA_{DIC}}\right) * (1 - e^{-\alpha_2 t}))}{\alpha_2} \quad (13)$$

V_t is the total rate of C_i uptake, f is the fraction of uptake attributable to CO_2 . HCO_3^- uptake was calculated as $1-f$. α_1 and α_2 are the temperature-, salinity-, and pH-dependent first order rate constants (uncatalyzed) for CO_2 and HCO_3^- hydration and dehydration, respectively (calculated as described by Espie and Colman (1986) with temperature and salinity corrections derived from Johnson, 1982).

Gene expression analysis

RNA sampling & extraction - For gene expression analysis, samples of $\sim 1.5 \times 10^7$ cells each were concentrated by filtration (1.2 μm polycarbonate filters, Millipore), the remaining culture were pelleted by 5 minute centrifugation at 600 g (Mikro 22R centrifuge, Hettich, Beverly, USA) and subsequently resuspended in RLT Buffer (Qiagen, Hilden, Germany) containing 14.3 mM β -mercaptoethanol (Sigma, Munich, Germany) prior to snap-freezing in liquid nitrogen and storage at -80°C . Cell disruption was performed with a TissueLyzer II beadmill (Qiagen, Hilden, Germany) after addition of 100 μL of glassbeads (\varnothing 0.1mm). Lysate was homogenized using QIAshredder spin-columns (Qiagen, Hilden, Germany) to breakdown macromolecular complexes prior to extraction.

RNA extraction was performed using a modified guanidinium thiocyanate method in combination with a silica-membrane-based separation technique (RNeasy mini kit, Qiagen). According to the manufacturer's manual, an on-column DNaseI digestion (Qiagen) was implemented to assure absence of DNA in the isolate. 7 Kunitz units of DNaseI (Qiagen, Hilden, Germany) were applied to the silica matrix following 20 minute incubation at room temperature. For further RNA cleanup MicroCon YM 30 ultrafiltration columns were used, following the manufacturer's protocol.

Microarray hybridization

RNA concentration and purity were measured photometrically with a Nanodrop ND1000 (PeqLab, Erlangen, Germany) and integrity of the isolate was assessed using a BioAnalyzer 2100 (Agilent, Santa Clara, USA) running an RNA 6000 Nano LabChip (Agilent). 200ng of integer isolate were spiked with RNA mixtures of known concentration (RNA Spike-In Kit, Agilent). These mixtures contain several RNAs of known concentrations which will cohybridize in known ratios to dedicated probes on the array. These ratios function as internal standards for normalization and as benchmarks of hybridization performance. Spiked RNA mixes were reversely transcribed using the low RNA input linear amplification kit (Agilent). Synthesis of cDNA was primed with T7-Promoter coupled oligo-dT primers. To increase the yield of longer transcripts,

SuperScript III reverse transcriptase (Invitrogen, Karlsruhe, Germany) was added to the reaction and the incubation protocol was correspondingly extended with an additional incubation at 50°C for 30 minutes prior to heat-inactivation of the enzymes.

In vitro transcription/amplification was carried out with T7 RNA Polymerase included in the kit, incorporating either Cy3 or Cy5 labeled CTP (Perkin Elmer, Waltham, USA) into the newly produced cRNA. Concentration and purity of produced cRNA as well as labeling efficiencies of the reactions were assessed photometrically (NanoDrop, Peqlab). Labeling efficiencies were calculated as [pmol dye/ng cRNA] from the results of photometry. Samples exhibited labeling efficiencies of 0.013 – 0.018 pmol dye (ng cRNA)⁻¹, which were all above the minimum required labeling efficiency 0.008 recommended by the manufacturer. Therefore all amplified cRNAs could be used in hybridization.

250 ng of each differently labeled and amplified cRNA was hybridized to 4x44K *Emiliana huxleyi* custom-built microarrays (Agilent). Microarray probes were derived from EST data compiled from the *E.huxley* CCMP1516 genome-project conducted by the US department of energy Joint Genome Institute (<http://www.jgi.doe.gov/>) in collaboration with the user community (Probe design and chip layout by Dr. Uwe John, AWD). Hybridization experiments were done in biological triplicates according to the hybridization scheme presented in Fig 8.

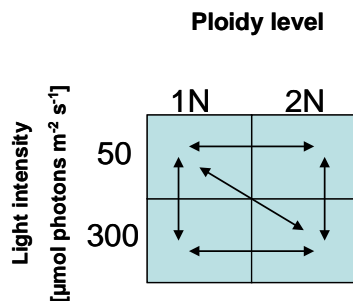


Fig. 8: Hybridization scheme of Microarray experiments; horizontal hybridizations are supposed to reveal ploidy-related effects on low-light and high-light acclimated cultures; Vertical hybridizations shall indicate irradiance effects on haploid and diploid cultures. In the diagonal hybridization both ploidy- and irradiance related effects should be visible, therefore it is used as a control.

Arrays were hybridized according to the Two-Color Microarray-Based Gene Expression Analysis protocol (Agilent) for 16 h at 64°C with an agitation of 6 rpm. in a hybridization oven (Rausfinden welche firma!). Arrays were scanned in a G2505B Microarray Scanner (Agilent) using standard photomultiplier tube (PMT) settings and 5µm scan resolution.

Feature evaluation

The dataset was normalized with Feature Extraction Software 9.0 (Agilent) using the locally weighted scatterplot smoothing (LOWESS) algorithm based on internal spike-in standards. Gene expression analysis was performed using the MultiExperiment Viewer 4.2 (MEV), which is part of the TM4 Software suite (Saeed et al. 2003; www.tm4.org).

Triplicate experiments were statistically evaluated in single class tests using the “significance analysis of microarrays” (SAM) algorithm introduced by Tusher et al. (2001). The datasets were permuted for 500 times each and gene regulation was called significant when gene-specific q-values (Storey et al. 2001) were ≤ 0.1 %. The q-value concept is an approach of Bayesian statistics: The results obtained from the experiments are compared to the fictive datasets generated by permutations. Posterior probabilities are then calculated for every analyzed gene to judge the probability of it being a false positive discovery. The q-value can therefore be seen as a bayesian analogue to the p-value and interpreted as a measure of test sharpness.

Clusters of significant genes were analyzed using Access 2003 Database software (Microsoft). Discovered significant genes were annotated using classifications of eukaryotic orthologous genes (KOG) which were provided by the US Department of Energy Joint Genome Institute (<http://www.jgi.doe.gov/>). Acquired gene sets were manually evaluated towards key enzymes or expression patterns, that may give hints towards certain metabolic or cytobiological pathways present in either haploid or diploid cultures, respectively.

Results

Acclimation dependent parameters - Growth rates of haploid (1N) and diploid (2N) cultures (Fig. 9) differ significantly with light conditions (ANOVA, $p < 0.05$, $F = 100.65$, $N = 204$). Growth rates in the high light treatments (HL) exceed those of the low light treatments (LL) by 37% and 62% in haploid and diploid cultures, respectively. Growth rates of the haploid cultures exceed those of the diploid cultures by 38% and 17% in low light and high light treatments, respectively.

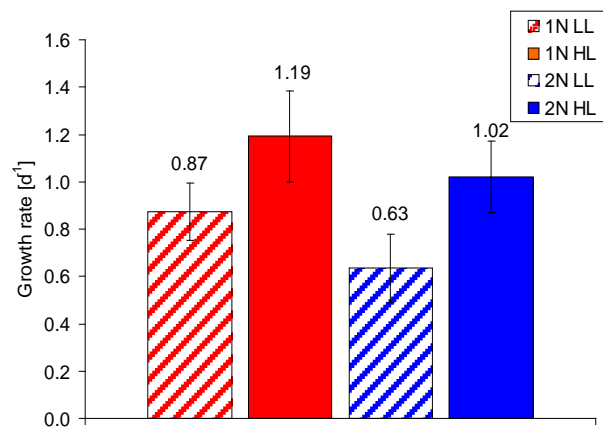


Fig. 9: Growth rates under the different treatments

Cellular content of organic carbon (Fig. 10) differed with light conditions. The haploid and diploid high light treatments showed 25% and 92% higher values than the respective low light acclimations. Haploid and diploid low light treatments did not differ significantly in POC content, whereas significant difference of the haploid and diploid high-light treatments was confirmed by one-way ANOVA ($p < 0.05$, $F = 4.27$, $N = 57$).

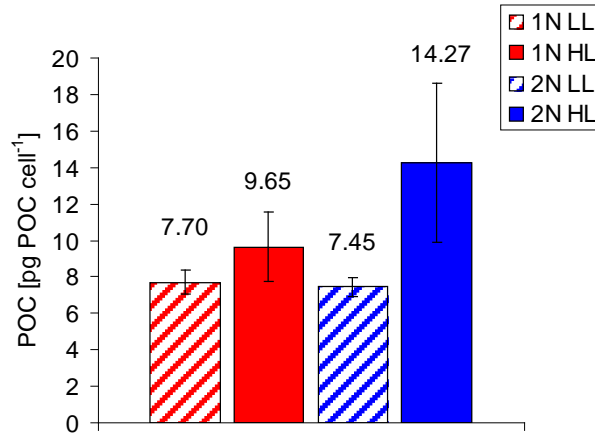


Fig. 10: Cellular POC contents under the different treatments

The daily POC production rates (Fig. 11) show 71% and 208% higher biomass accumulation in high light compared to low light of haploid and diploid cultures, respectively. In the low light acclimated cultures the haploid stages build up more POC per day, due to the higher growth rate.

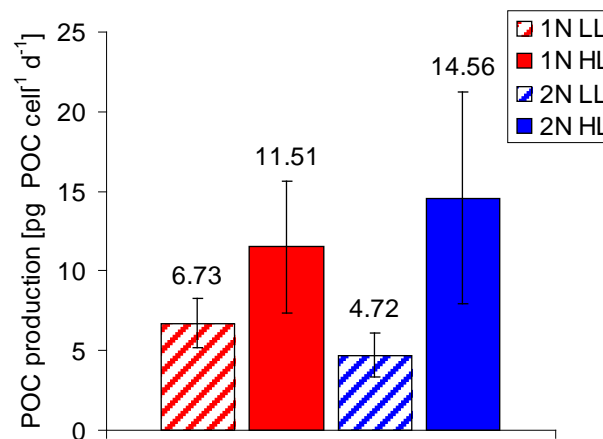


Fig. 11: POC production under the different treatments

Cellular contents of PIC (Fig. 12) were near zero for the non-calcifying haploid cultures. In the calcifying diploid cultures, PIC content of the low light treatment exceeds the high light treatment's PIC content by 25%. This difference in PIC content is however statistically not significant as tested by one-way ANOVA ($p > 0.05$, $F = 3.29$, $N = 13$).

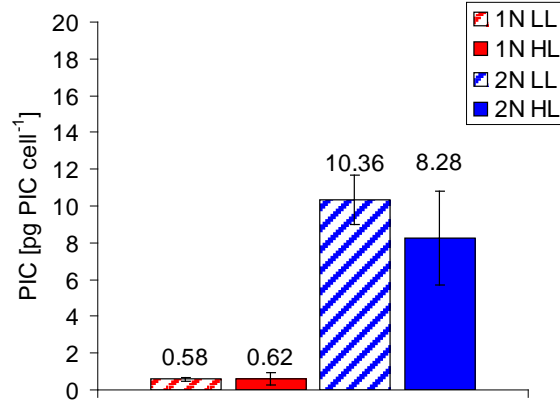


Fig. 12: Cellular PIC contents under the different treatments

The daily PIC production (Fig. 13) reflects that haploid cultures exhibit PIC buildup rates near zero. Within the diploid cultures the production of CaCO₃ is moer or less different.

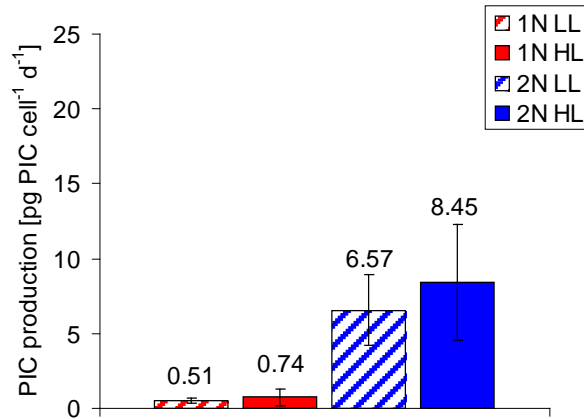


Fig. 13: PIC production under the different treatments

The PIC:POC ratios (Fig. 14) of haploid cultures are below 0.1. PIC:POC ratio of the diploid low light acclimated cultures reveal, that inorganic carbon comprises 58% of total carbon. In the high light treatment of the diploid culture the contribution of inorganic carbon to total carbon is only 32%.

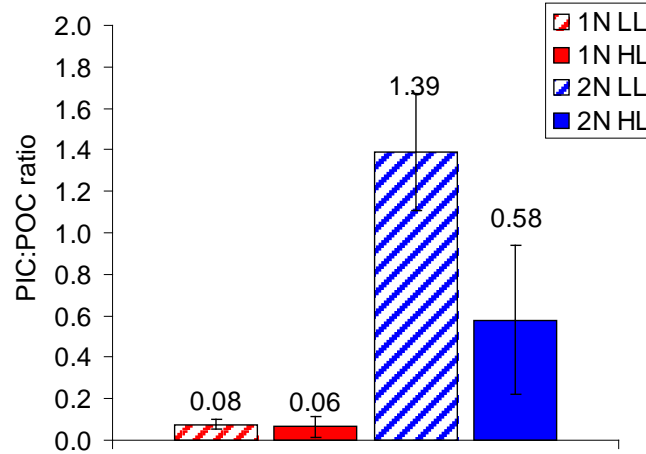


Fig. 14: PIC:POC ratios in the treatments

Cellular content of PON shows tendency to correlate with growth rate, being 16% and 22% higher in the high light treatments of haploid and diploid cultures than in the respective low light treatments (Fig. 15). Means are significantly different according to one-way ANOVA ($p < 0.05$, $F = 4.27$, $N = 57$).

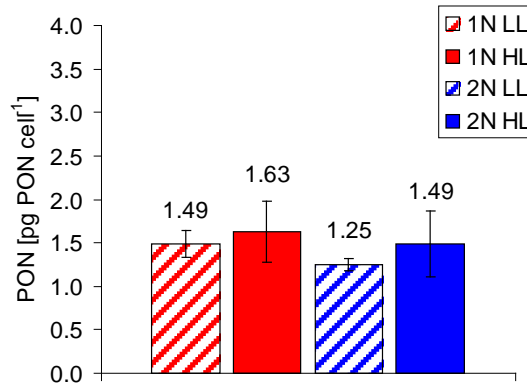


Fig. 15: Cellular Contents of PON in the treatments

Daily PON production rates (Fig. 16) are 49% and 92% higher in the high light acclimated haploid and diploid cultures respectively. Comparing ploidy levels, the haploid cultures produce slightly more PON per day (64% and 28% in low light and high light acclimated cultures, respectively).

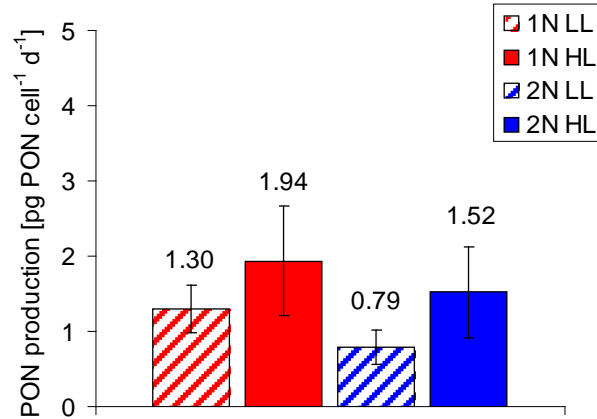


Fig. 16: PON production rates under the different treatments

Within the haploid and diploid cultures the elemental ratios of C:N (Fig. 17) change with acclimation light intensity, increasing 16% and 25% under high light in haploid and diploid cultures, respectively. Comparing the life-cycle stages, C:N ratios are generally higher in the diploid cultures.

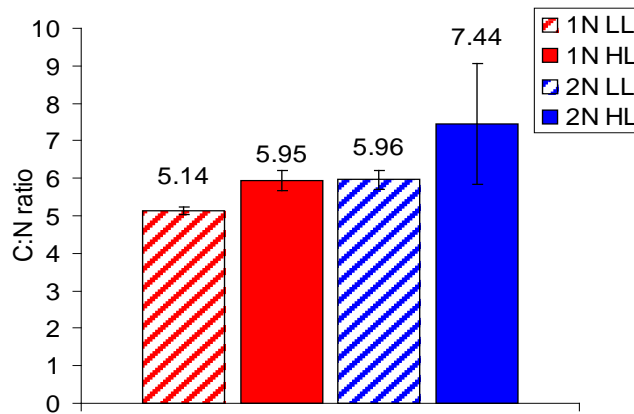


Fig. 17: Elemental ratios of C:N in the different treatments

Chlorophyll a contents (Fig. 18) are generally higher in the low light acclimated cultures, exceeding the respective high light adapted cultures by 111% and 33% in the high light acclimated haploid and diploid cultures respectively (Significant according to one-way ANOVA, $p < 0.05$, $F = 30.0$, $N = 31$). Comparing the cultures, the haploid low light cultures build up more Chl *a* than respective diploid cultures. In contrast, in the high light treatments the diploid cultures build up more Chl *a*, than the haploid cultures.

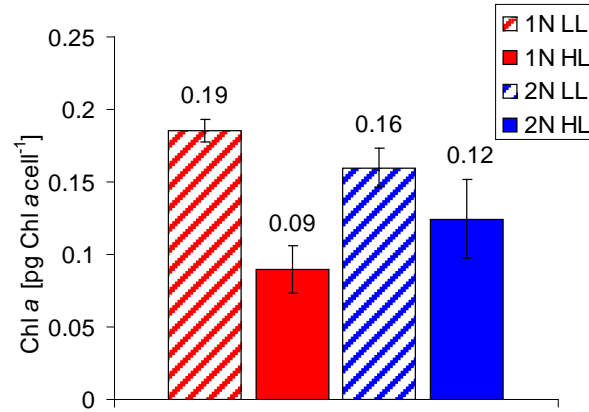


Fig. 18: Chl *a* contents of the different treatments

The Chl *a*:POC ratio reveals equal fractions of Chl *a* per biomass in the light treatments (0.001 in both low light treatments, Fig. 19). In the high light treatments chlorophyll fractions are 0.024 and 0.021 in haploid and diploid cultures, respectively.

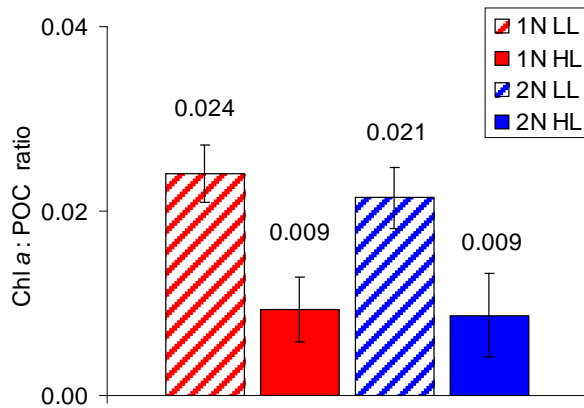


Fig. 19: Chl *a*:POC ratios of the different treatments

Isotopic analysis data yielded a higher isotope fractionation during formation of organic matter in the high light cultures (6.1‰ and 1.05‰, Fig. 21). Comparing the ploidy stages, slightly higher isotope fractionation can be observed in the haploid cells.

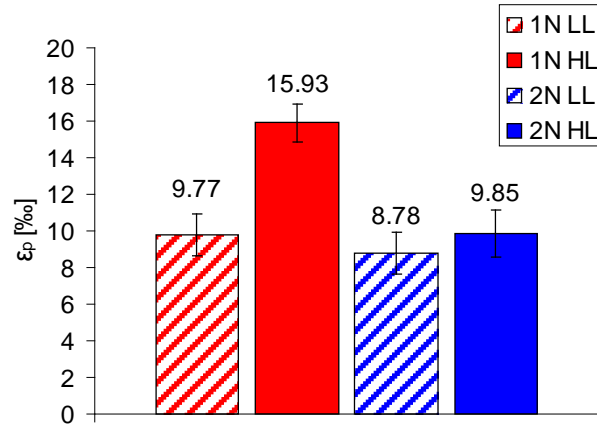


Fig. 20: Isotope fractionation during biomass accumulation

Bioassays

Photosynthesis vs. irradiance - Results of photosynthesis-irradiation assays (Fig. 21, Tab. 4) show that the diploid cultures exhibit roughly 70% higher maximum photosynthetic O₂ evolution (V_{max}) when normalized to Chl *a*. Within the life-cycle stages respective maximum rates did not differ significantly. The compensation points (K_p) were generally lower in the low light acclimations. K_p values of the high light treatments exceed the K_p of the low light treatments by 240% and 66% in haploid and diploid cultures, respectively. Initial light limited slopes (α) are 18% and 60% steeper in the low-light acclimated haploid and diploid cultures, respectively. Light acclimation indices (I_k) of the low light acclimated cultures are generally lower (137 and 70 $\mu\text{mol photons m}^{-2} \text{s}^{-1}$) than those of the high light treatments (247 and 186 $\mu\text{mol photons m}^{-2} \text{s}^{-1}$) of the haploid and diploid cultures respectively. It can be seen, that the I_k values of the haploid and diploid stage are above acclimation light intensity in the low light treatments and below acclimation light intensity in the high light treatment. It has to be noted, that in the low light treatments, the I_k of the haploid stage is much higher above the acclimation light intensity than the diploid stage's. In the high light treatments in contrast, I_k values of the haplonts are lower than those of the diploid stages'.

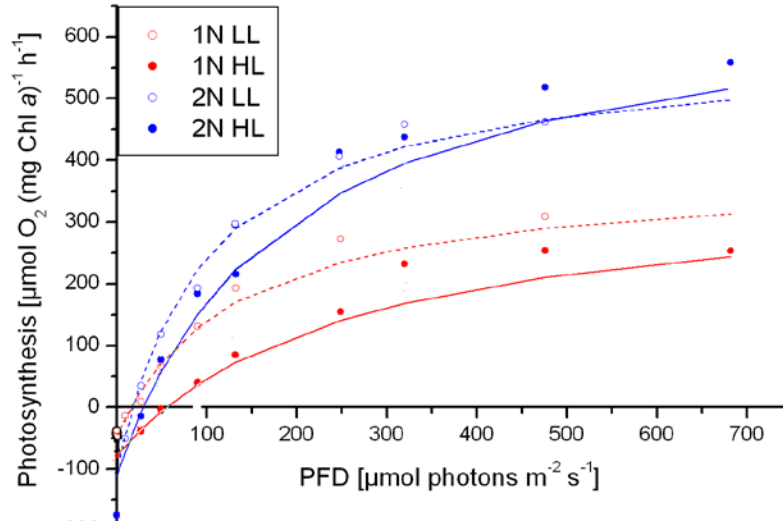


Fig. 21: Chlorophyll-normalized photosynthesis-irradiance plots, one representative dataset per treatment was drawn.

Tab.4: Key parameters of photosynthesis vs. irradiance assays (Chl a normalized); V_{\max} : Maximum O₂ evolution rate [$\mu\text{mol O}_2 (\text{mg Chl a})^{-1} \cdot \text{h}^{-1}$]; K_p : Compensation point [$\mu\text{mol photons m}^{-2} \text{s}^{-1}$]; α : Initial light-limited slope [$\mu\text{mol O}_2 (\text{mg Chl a})^{-1} \text{h}^{-1} (\mu\text{mol photons} \cdot \text{m}^{-2} \cdot \text{s}^{-1})^{-1}$]; I_k : Light acclimation index [$\mu\text{mol photons m}^{-2} \text{s}^{-1}$]

	V_{\max}	K_p	α	I_k
1N LL	380 ± 48	16 ± 4	3.0	137
1N HL	364 ± 47	54 ± 7	1.5	247
2N LL	584 ± 31	17 ± 2	8.4	70
2N HL	685 ± 63	29 ± 5	3.7	186.

Photosynthesis vs. DIC and CO₂ - Maximum photosynthetic O₂ evolution (Fig. 22 A and B) were generally higher in high light adapted cultures, exceeding the V_{\max} of the low light acclimations by 329% and 194% in haploid and diploid cultures respectively. Note that the diploid high light acclimated cultures exhibited a decrease in photosynthetic rate with increasing DIC and CO₂.

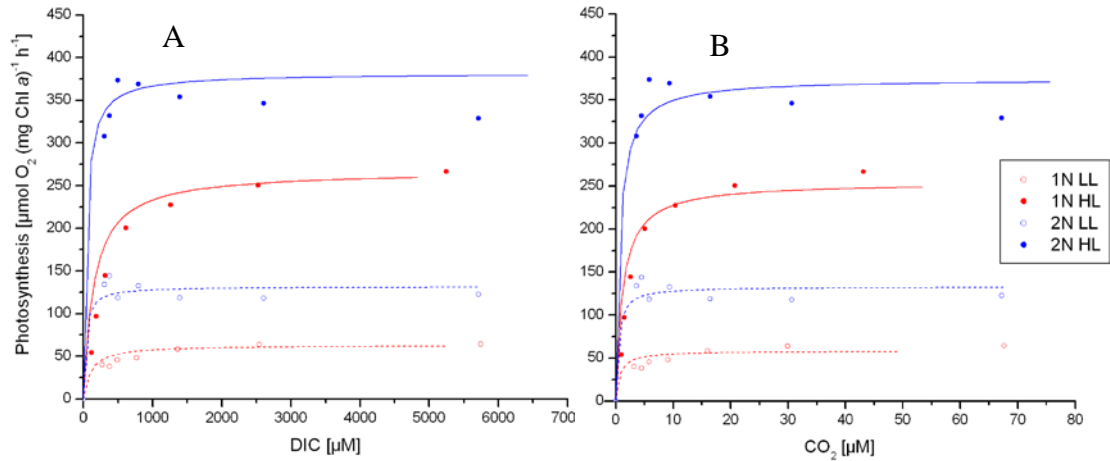


Fig. 22: Chl a normalized photosynthesis vs. DIC (A) and CO₂ (B) , one representative dataset per treatment was drawn

Tab. 5: Key parameters obtained from photosynthesis vs. DIC assay (Chl a normalized); V_{\max} : Maximum O₂ evolution rate [$\mu\text{mol O}_2 (\text{mg Chl a})^{-1} \text{h}^{-1}$]; $K_{1/2 (\text{DIC})}$: Half-saturation constant for DIC [μM]; $K_{1/2 (\text{CO}_2)}$: Half-saturation constant for CO₂ [μM]

	V_{\max}	$K_{1/2 (\text{DIC})}$	$K_{1/2 (\text{CO}_2)}$
1N LL	58 ± 2	62 ± 14	1 ± 0
1N HL	251 ± 13	102 ± 26	1 ± 0
2N LL	125 ± 4	N/A	N/A
2N HL	378 ± 2	N/A	N/A

¹⁴C disequilibrium experiments - The ¹⁴C disequilibrium assay showed that *E.huxleyi* predominantly uses HCO₃⁻ as the inorganic carbon source (Fig. 23A). Since one-way ANOVA negate significance ($p > 0.05$, $F = 2.6$, $N = 12$), the differences between high light and low light acclimations can not be properly interpreted as light effects. Slightly higher apparent HCO₃⁻ contribution in the control indicates the presence of eCA activity (one-way ANOVA, $p < 0.05$) in both haploid and diploid life-cycle stages (Fig. 23B). Significance was approved by one-way ANOVA ($p < 0.05$, $F = 5.95$, $N = 12$).

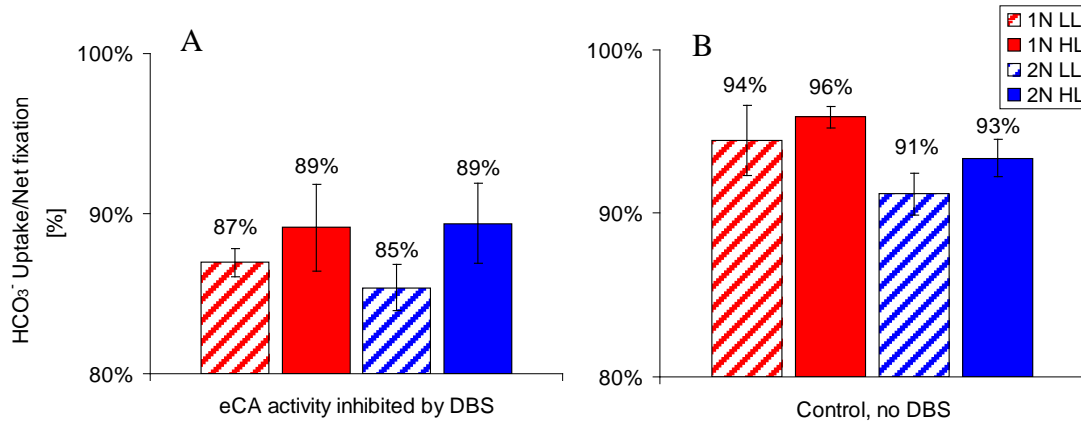


Fig. 23 A: Active HCO₃⁻ uptake, contribution to net fixation; 23B: HCO₃⁻ contribution to net fixation with uninhibited eCA

CA assay using MIMS - Though CA assessments using the MIMS approach (Figs 24A and 24B) indicate presence of eCA in all treatments, in comparison to the low light acclimated cultures, the haploid and diploid high light cultures exhibit 115% and 223% higher eCA activity, respectively (One-way ANOVA, $p < 0.05$, $F = 21.13$, $N = 13$). Comparing the ploidy levels, low light and high light acclimated cultures show 733% and 456% higher activity in the haploid stage, respectively, indicating significantly higher activity of eCA in the haploid stage (Fig. 24A). Assessments of iCA (Fig. 24B) do not indicate a light-dependent increase in activity in haploid but in diploid cells: While in haploid cells the iCA activities remain fairly constant, in diploid cells there is a significant increase of 253% due to the higher light intensity.

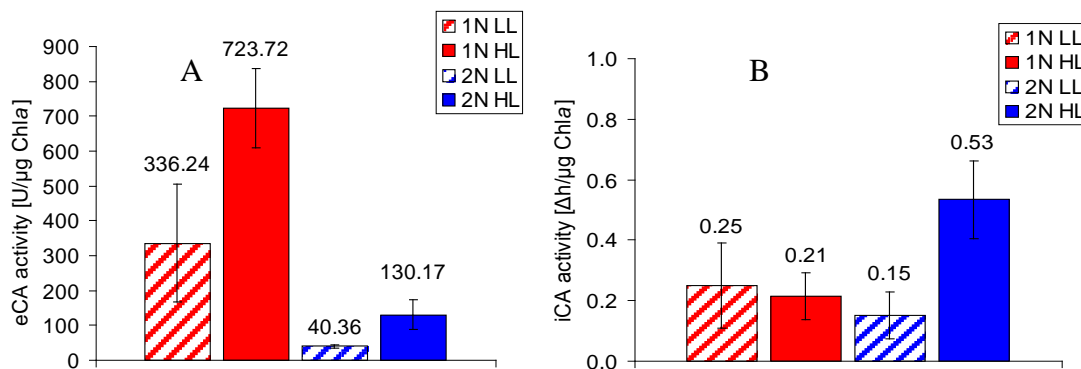


Fig. 24A: Activities of eCA in the treatments B: Activities of iCA in the treatments

Gene expression analysis - Results of gene expression analysis report 2449 and 1840 genes that are specifically up- and downregulated in the diploid life-cycle stage (i.e. correspondingly down- and upregulated in the haploid stage). These genes were also verified by the control experiments (Fig. 25), whereas light intensity related effects (Fig. 26) could not be observed.

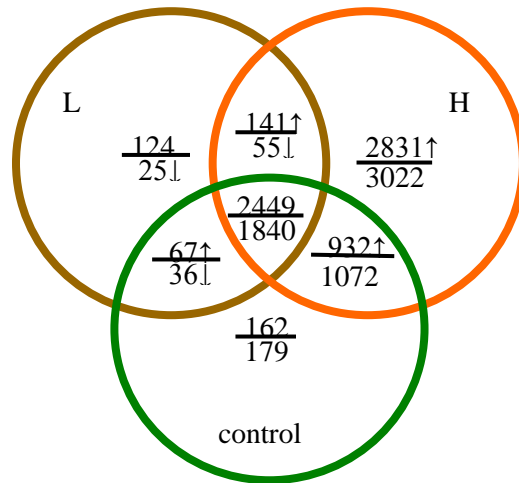


Fig. 25: Transcriptomic responses on life-cycle transition discovered in the low light (brown), high light (orange) and control (green) hybridizations; ↑ = upregulated in 2N, ↓ = downregulated in 2N (= upregulated in 1N). Central intersection represents the acquired gene set, attributable to ploidy effects:

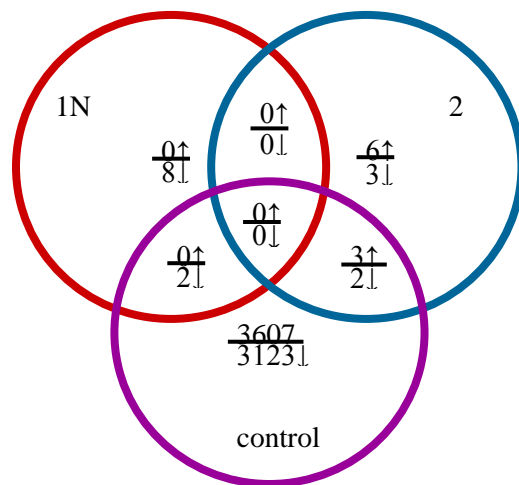


Fig. 26: Transcriptomic responses on acclimation light intensities discovered in the haploid (red), diploid (blue) and control (purple) hybridizations; ↑ = upregulated in high light, ↓ = downregulated in low light (= upregulated in high light).

Genes responding to ploidy changes are presented in table 6. A full list of discovered genes can be found in the appendix.

Tab. 6: Upregulated genes in 1N and 2N cultures of *E. huxleyi*

KOG classification	1N ↑	2N ↑
Amino acid transport and metabolism	19	28
Carbohydrate transport and metabolism	23	23
Cell cycle control, cell division, chromosome partitioning	4	8
Cell motility	3	3
Cell wall/membrane/envelope biogenesis	7	9
Chromatin structure and dynamics	17	6
Coenzyme transport and metabolism	0	8
Cytoskeleton	37	98
Defense mechanisms	1	3
Energy production and conversion	20	27
Extracellular structures	23	18
Function unknown	30	43
General function prediction only	114	82
Inorganic ion transport and metabolism	28	20
Intracellular trafficking, secretion, and vesicular transport	10	17
Lipid transport and metabolism	9	20
Nuclear structure	1	5
Nucleotide transport and metabolism	0	6
Posttranslational modification, protein turnover, chaperones	35	47
Replication, recombination and repair	5	14
RNA processing and modification	28	10
Secondary metabolites biosynthesis, transport and catabolism	7	13
Signal transduction mechanisms	78	72
Transcription	48	44
Translation, ribosomal structure and biogenesis	20	9
No data	1273	1816
TOTAL	1840	2449

The diploid cultures exhibit strong expression of genes important for cellular microtubuli-related trafficking machinery (>50 genes for tubulin subunits and associated molecular motors Kinesin/Dynein). A larger and more variable set of genes involved in posttranslational modifications has been found in the diploid cultures (18 genes in 1N versus 40 genes in 2N after subtraction of “housekeeping” DnaJ heatshock proteins).

The haploid cultures in contrast exhibit a strong expression of genes related to the formation of clathrin coated vesicles (Vesicle coat complexes, adaptor proteins and auxilin, an assembly assist protein). Moreover vacuolar activity seems to play an important role in the haploid stage, due to the high expression levels of vacuolar H⁺ ATPases (13 genes related to different subunits). Further 3 genes were found related to vacuolar sorting and another 5 genes involved in vacuolar protein degradation were found.

Considering genes important for the process of gene expression itself, a high regulation of initiation, RNA modification, and transcription was found in haploid cultures, involving 29 genes related to splicing machinery and 47 genes related to the transcription and its regulation in contrast to only 10 and 9 respectively in diploid cultures. The diploid culture in turn exhibited upregulation of genes related to post-translational modifications and to ubiquitin mediated protein turnover.

Discussion

Acclimation responses

Obtained growth rates of the TQ26 strain (Fig. 9) were found to be similar to those reported from studies with cultured *E.huxleyi* strain PML B92/11, in which growth rates (μ) ranged from 0.66 d^{-1} [PFD $30 \mu\text{mol photons m}^{-2} \text{ s}^{-1}$] to 1.1 d^{-1} [PFD $180 \mu\text{mol photons m}^{-2} \text{ s}^{-1}$] (Rost *et al.*, 2002). In the present study, growth rates obtained in haploid cells were generally higher, than in the diploid cultures. This phenomenon, which has thus far not been described, can most probably be attributed to the fact that the smaller haploid cells enter cell-cyclic S phase earlier, i.e. with lower biomass, as cell size is the common trigger for G1-to-S transition (Lodish *et al.*, 2008). It could also be argued that calcification demands energy at the expense of growth.

Calcifying diploid cells exhibit equal or higher cellular POC content (Fig. 10) and thus in terms of POC production (Fig. 11) do not seem to be adversely affected by calcification. POC production itself did not differ significantly between life-cycle stages but with acclimation light intensity due to higher photosynthetic activity.

Cellular PIC content is near zero in haploid cultures (Fig. 12), confirming absence of calcification in this life-cycle stage. The lack of calcification was also visually verified using light-microscopy. Because PIC is calculated as the difference between TPC and POC, small putative PIC contents may therefore be attributed to uncertainties in analyses (0.2 pg). Diploid cells clearly show calcification, cellular PIC contents being highest in low light acclimated cultures. Concerning the PIC production, daily calcite buildup is more or less equal, and thus the differences in calcite content originate from faster growth (Fig. 12). From this it can be concluded that PIC production is less sensitive to changes in light intensity when compared to processes like growth and POC production (Trimbornet *et al.*, 2007)

The *degree* of calcification is often expressed by the PIC:POC ratio (Fig. 14). It has to be noted that the degree of calcification strongly depends on growth rate and not only PIC production. Hence, higher PIC:POC ratios, as observed here under low light, reflect limitation in growth and photosynthesis rather than stimulation in calcification. Similar effects on PIC:POC have also been observed for P and N limited cells of *E. huxleyi*

(Paasche, 2002). Cells with multiple layers of coccoliths due to decreased division rates in stationary phase have for example been reported by Linschooten *et al.* (1991). PON contents of cells were shown to increase with increasing light intensity but did not differ between life-cycle stages (Fig. 15). Since increased light intensity results in higher growth rates, daily PON production shows the same pattern in an even amplified manner (Fig. 16). This may be due to the efficiency of nitrogen assimilation machinery, especially the activity of nitrate reductase. This first enzyme in the assimilation pathway from nitrate (NO_3^-) to glutamine is being strongly dependent on reduction equivalents in form of NAD(P)H and therefore being governed by acclimation light. The C:N ratios of acclimated cultures increased with light intensity (Fig. 17), which reflects larger increase in POC than in PON content with light. The high C:N ratios of diploid cultures can be attributed to higher POC content, possibly due to increased storage of carbohydrate. Lower C:N ratios of the haploid cultures, in turn, might derive from reduced buildup and storage of carbohydrate as a result of accelerated growth (Fig 9). The observed higher and lower Chl *a* contents are a common response to the decreased or increased acclimation light intensities (Fig. 18; Falkowski & LaRoche, 1991). Obtained values were comparable with an earlier study on light acclimation of calcifying *E. huxleyi* (Nielsen, 1997). Since cells of haploid cultures are smaller and therefore have lower POC content, cellular Chl *a* quotas are difficult to compare to quotas of diploid cells. Normalization to biomass yields the Chl *a*:POC ratio, which indicates similar Chl *a* contents in relation to overall biomass in the high light acclimated cultures (Fig. 19).

Bioassays

Photosynthesis vs. irradiance - Maximum rates of photosynthetic O₂ evolution (V_{max}) are generally higher in 2N cultures than in 1N cultures. The V_{max} values obtained from the curve fitting procedure roughly correspond to those obtained by Nielsen (1997), who investigated light acclimation over a range of light levels and day lengths in a diploid strain of *E.huxleyi*. Obtained α values are significantly higher than those described by Nielsen. This may be attributed to the fact that the modified Michaelis-

Menten equation used for the curve fitting procedure does not level out near saturation light intensities. The equation was chosen since alternative mathematical equations, e.g. Jassby & Platt (1976), described the obtained data even less well: The latter function stringently implements photoinhibition and does not account for the fact that net and not gross photosynthesis is measured, and as a result lacks a compensation point. A weakness of the used Michaelis-Menten equation may, however, be reflected in the apparent overestimation of V_{\max} . In the present study, high light and low light acclimated treatments exhibit nearly equal V_{\max} values under same light intensities (Fig. 21). Moreover, cells of the low light treatments reach saturation at lower PFDs, as indicated by higher α and lower I_k , and there is no sign of photoinhibition over the investigated PFD range. Interestingly, I_k values of low light cultures were generally higher than acclimation intensities, whereas the high light cultures exhibited I_k values below acclimation level. These findings suggest a higher degree of flexibility in the low light cultures towards changes in the light regimes. In other words, small changes in PFD will result in large responses of photosynthetic activity. The earlier saturation in the high light cultures, in contrast, might be interpreted as species-specific threshold beyond which responses in photosynthetic rates result in significantly smaller responses in cells of this treatment.

Concerning the ploidy effect, diploid cultures exhibit generally higher initial light-limited slopes (α) and lower I_k values, thus will reach light saturation at lower PFDs than the haploid cells. Moreover, maximum photosynthetic rates of diploid individuals are higher, thus they may be able to outcompete haploid individuals, independent of respective light acclimation.

Photosynthesis vs DIC/CO₂ - Photosynthesis vs. DIC/CO₂ plots show high apparent affinities for inorganic carbon in both life-cycle stages: Haplonts and diplonts exhibit half saturation constants for DIC and CO₂ smaller than those of RubisCO (20-70 μ M, Badger *et al*, 1998), suggesting the operation of a CCM in the first instance. From the plots it can be seen, that low light acclimated cultures are more affine, consistently reaching saturation levels earlier than the diploid cultures of the same light acclimation

(Fig. 22A and B). $K_{1/2}$ (DIC) values determined for the haploid cultures were $62 \pm 14 \mu\text{M}$ and $102 \pm 26 \mu\text{M}$ in LL and HL treatments, respectively. $K_{1/2}$ (CO_2) values determined for the haploid cultures were 0.64 and $1.16 \mu\text{M}$ in the low and high light treatments. Values for the diploid cultures could not be obtained due to initially high DIC concentrations.

The obtained half-saturation constants for the low light treatments are lower than those obtained from Nimer & Merret (1996, 1997) who reported $K_{1/2}$ (DIC) and $K_{1/2}$ (CO_2) values of $200 \mu\text{M}$ and $1.6 \mu\text{M}$ respectively. Other authors (e.g. Paasche, 1964; Rost *et al.*, 2003, 2006), have reported much higher $K_{1/2}$ (CO_2) of 6-27 μM for a calcifying strains of *E.huxleyi*. Since affinities were strongly altered with growth conditions, for instance the acclimation pCO_2 , it was concluded that a lowly-efficient but highly-regulated CCM operates in *E.huxleyi*. The difference between this and previous studies is that Rost *et al.* (2003, 2006) used a disequilibrium approach and therefore inhibited eCA activities, while in the present approach CA was added to ensure full equilibration between CO_2 and DIC. Although this can have contributed to the different findings, it is more likely that strain-specific differences in terms of affinities do exist.

Photosynthesis rates obtained at concentrations of $\sim 2.1 \text{ mM DIC}$ ($\sim 20 \mu\text{M CO}_2$) and acclimation light intensity are consistent with the rates obtained in the photosynthesis vs. irradiance assays. Combining the results of both assays it can be said, that under equal [DIC], diploid cells exhibit significantly higher photosynthesis rates, regardless of PFD. These differences in maximum rates correspond well to the differences observed in POC production (Fig. 11). Furthermore both stages have a high affinity for DIC, so that this strain might not be limited in today's ocean, as often stated for many other less affine strains (Rost & Riebesell, 2004 and references therein).

Determination of photosynthetic carbon source - The ^{14}C disequilibrium assay showed a high HCO_3^- contribution to net fixation in both, haploid and diploid *E.huxleyi* cells, indicating direct uptake mechanisms for this carbon species (Fig. 23A). These findings are inconsistent with results of Elzenga *et al.* (2000), who report CO_2 to be the source

for carbon fixation in a coccolith forming *E. huxleyi*. As stated by Trimborn et al. (2008), incorrect rate constants were used in this particular study. An overestimation of α could have therefore resulted in a possible underestimation of the HCO_3^- contribution (Rost *et al.*, 2007). The high HCO_3^- contribution in both life-cycle stages argues strongly against the hypothesis, that HCO_3^- uptake and the subsequent use in photosynthesis is functionally coupled to calcification. Calcification obviously does not represent a mean for HCO_3^- uptake as the non- calcifying haploid cells showed equally high HCO_3^- uptake relative to net fixation. The fact of active HCO_3^- uptake may however contribute to the high apparent affinities for inorganic carbon detected in the photosynthesis vs. DIC assay.

Fractionation and carbon fluxes - The ϵ_p of the diploid cultures is in the range of ϵ of 8-10‰ (Fig. 21), which corresponds to values observed by Rost *et al.* (2002) under similar conditions. The higher fractionations of the haploid cultures (~10-16‰) indicate a higher loss of inorganic carbon due to cellular leakage. To investigate this phenomenon, the relative contribution of HCO_3^- uptake and obtained fractionation data were used to calculate the cellular CO_2 leakage (Fig. 28)

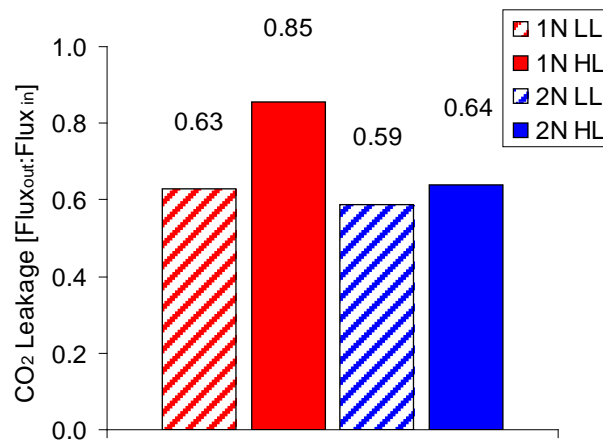


Fig. 28: CO₂ leakages of the treatments, calculated based on the model of Sharkey & Berry (1976)

Calculation results show, that both life-cycle stages exhibit high leakages of CO₂. In the high light haploid cultures the effect is even larger. The increase in leakage with irradiance observed in this strain can be attributed to higher HCO₃⁻ pumping activity relative to C fixation, as was suggested by Rost et al. (2002). Since HCO₃⁻ contribution to net fixation stays equal, as seen from the ¹⁴C data, the higher leakage must be attributed to increased C_i uptake due to higher transport activity, implicating the CCM to work in a light dependent manner. Further, though less probable, different membrane properties of the haplonts stage could be responsible for the increase in leakage of imported inorganic carbon

CA activities - Activities of eCA in the diploid stages were low (40-130 U/μg Chl *a*) which corresponds to earlier findings of Rost et al. (2003). Activities of eCA in haploid *E.huxleyi* cells were significantly higher (336-723 U/μg Chl *a*) (Fig. 23A). The MIMS-based CA assessment could not detect considerable activities of eCA in diploid cells, whereas the comparison of DBS and control run of ¹⁴C disequilibrium technique suggested eCA activity in both life-cycle stages (Fig. 22 B). This might be attributed to the fact, that although the disequilibrium approach is a very robust assay for measuring proportions of C_i usage, an accurate estimation of eCA is becoming increasingly biased when organisms exhibit high rates of HCO₃⁻ usage in carbon acquisition (Rost et al., 2007). Therefore the results of the MIMS-based assays are taken as more trustworthy, indicating significant presence of eCA activity in the haploid stage

The common notion, that eCA is involved in indirect bicarbonate utilization by conversion of HCO₃⁻ to CO₂, which could then be transported through the plasma membrane and used for photosynthesis (Elzenga et al. 2000, Sültemeyer 1998, Tortell et al. 2006) is not supported by the results. The correlation of eCA activity with direct HCO₃⁻ uptake observed in the haplonts (Fig. 22), rather suggest a C_i recycling mechanism as proposed by Trimborn et al. (2008). According to that, active carbon upake increases [CO₂] within the cells. The ability of CO₂ to permeate biomembranes will result in a certain degree of leakage, increasing pCO₂ in the vicinity of the cell. The decrease of overall [DIC] due to photosynthetic carbon fixation will also increase pH in

the vicinity of the cells, so that eCA will perform the conversion of leaked CO₂ into HCO₃⁻ which is readily taken up. This correlation of eCA activity and HCO₃⁻ usage was also reported in numerous phytoplankton species (Martin & Tortell, 2006).

Regarding iCA activity it has to be noted that this approach is semiquantitative and results are difficult to compare over tested species with different sizes and membrane properties. However, the obtained results (0.25-0.53 Δh/μg Chl *a*) are in the same range as those of *Phaeocystis globosa*, a prymnesiophyte well comparable with *E.huxleyi* in size (Rost et al., 2003). For qualitative and comparable results estimates, cells would have to be disrupted and total CA in the lysate would have to be compared to signals obtained from assessments of eCA. The role of iCA is, however, uncertain since there are several isoforms (cytoplasmic, mitochondrial, chloroplastic) with putatively different functions and/or locations.

Gene expression analysis - Analyses of the light responses revealed no obvious effects. cDNA synthesis, labeling, and hybridization were performed optimally. Array features were attributed to the annotated genes of the genome correctly after normalization and analysis. The used KOG data contained only few light relevant genes, but the lack of findings cannot be explained by this fact. However, the overall expression pattern was more or less unaltered. Therefore, it can be hypothesized, that the used light intensities do not impose stress to *E.huxleyi* and therefore did not significantly affect gene expression profiles. The observed results may therefore be attributed to post-translational modifications of proteins involved in photosynthesis. Whereas in the light treatment, effects on gene expression levels were not prominent, strong effects due to different ploidy stages were observed.

The haploid stage tightly regulates gene expression, probably for the benefit of rapid cell cycling as indicated by the higher growth rates (Fig 10). These findings suggest a rather parsimonious organismic organization. The diploid stage in contrast accumulates higher biomass (Fig. 12) and therefore might have demand to maintain high protein levels and turnover rates. This might be reflected in the high expression levels of genes related to ubiquitin-mediated protein degradation.

The strong expression of genes for microtubuli-related trafficking machinery in the diploid stage can to a large extent be attributed to the continuous export of coccolith vesicles. Linschooten et al. (1991) have found that coccoliths are produced with a rate of $\sim 1 \text{ h}^{-1}$ in the light phase, for which the corresponding machinery is required. Microtubuli and associated motor proteins are also essential for structure and function of the haplont's flagella. The lack of discovery of these proteins in the haploid stage does not implicate that the genes are absent or suppressed, rather the amount of transcript is significantly higher in the diploid stage.

The haploid phase exhibits a strong upregulation of genes related to the buildup and transport of clathrin coated vesicles; these vesicles have been shown to act in endocytosis of protists (Elde et al., 2005; Field et al., 2006). Although most haptophytes possess chloroplasts and therefore can be assumed to be photoautotrophs, some species, e.g. *Balaniger balticus*, and maybe other coccolithophores, appear to lack a photosynthetic apparatus (Marchant and Thomsen, 1994). It has further been shown that, in addition to photosynthesizing, some haptophyte species are capable of incorporating either dissolved organic carbon or particulate organic material, i.e., they are mixotrophic (Green, 1991; Jones et al., 1994; Tillmann, 2003).

The expression of vacuolar sorting machinery and numerous proteins involved in vacuolar digestion (proton pumps, various vacuolar proteases) strongly support mixotrophy in haploid *E.huxleyi*. Another interesting finding is the expression of a polyketide synthase (type I). These large multi-domain enzymes produce long-chain C-compounds from acetyl and propionyl precursors in a process similar to fatty acid synthesis (John et al., 2008). It has been shown that certain potent polyether biotoxins found in haptophytes are derived entirely or in part from this pathway (MacKinnon et al., 2006; Wright and Cembella, 1998). Numerous purposes are under debate, among them grazing avoidance, interspecific competition and signaling (John et al., 2008; Staunton & Weissman, 2001).

Conclusions & Outlook

The two life-cycle stages of *E.huxleyi* possess strikingly different properties: In addition to calcification, the diplont exhibits a higher photosynthetic performance than the haplonts in terms of O₂ evolution and POC accumulation. A broad spectrum of physiological methods was applied, to elucidate responses to acclimation conditions as well as processes of photosynthesis and carbon acquisition. It can be stated, that the diploid stage is able to use low light intensities more efficiently and reaches higher maximum rates of photosynthesis at lower photon flux densities. The haplont in contrast is able to react to a broader range of light intensities with a more flexible scaling of photosynthesis rates, allowing to avoid early light saturation. Regarding the modes of carbon acquisition, both life-cycle stages operate a highly-affine carbon concentrating mechanism (CCM) based on direct HCO₃⁻ uptake. Higher eCA activities and cellular leakage were derived in the haploid stage.

Concerning the molecular data of the haploid stage, it can be hypothesized, that the less efficient photosynthesis activity and the tight gene regulation interdepend. On this basis, it could be postulated for the diplont, that high photosynthetic rates and POC accumulation in turn demand high rates of gene expression and protein turnover. However, the results cannot explain the observed differences in photosynthetic performances between life-cycle stages. Molecular analyses suggest that the haploid life-cycle stage of *Emiliana huxleyi* exhibits an ancestral haptophyte life-style, involving flagella, mixotrophy and potential toxicity due to polyketide synthesis.

With respect to ecology, the results bear new implications for the haploid stage, which arises after viral affection of diploid populations. Being mixotroph, the haplonts may have the ability to profit from post-bloom-termination situations. Potential toxicity might support enduring dominance over other competing phytoplankton species in the environment.

Concerning further investigations on the findings, results of microarray analyses should be validated by means of quantitative RT-PCR, to quantify relative transcript abundances. The effects of other abiotic factors like CO₂/pH or nutrient availability have to be tested to further characterize the physiological capabilities of both life-cycle stages. To investigate the haplonts' ecological roles and niches, community- and grazing-

experiments have to be performed. Reactions to environmental conditions have to be assessed to connect physiological condition and potential toxin production. The combined data may provide information on the sensitivity of the life-cycles stages to global change and the succession dynamics of natural phytoplankton assemblages.

References

Anderson DM, Chisholm SW, Watras CJ: Importance of life cycle events in the population dynamics of *Gonyaulax tamarensis*, *Marine Biology* 76, 179-189 (1983)

Anning T, Nimer N, Merret MJ, Brownlee C: Costs and benefits of calcification in coccolithophorids, *J. Marine Sys.* 9, 45–56 (1996)

Armstrong RA, Lee C, Hedges JI, Honjo S, Wakeham SG: A new, mechanistic model for organic carbon fluxes in the ocean based on the quantitative association of POC with ballast minerals, *Deep Sea Res.*, 49(2), 219–236 (2002)

Badger MR, Price, GD: Carbonic anhydrase activity associated with the cyanobacterium *Synechococcus* PCC7942, *Plant Physiol.* 89, 51–60 (1989)

Badger MR, Andrews TJ, Whitney SM, Ludwig M, Yellowlees DC, Leggat W, Price GD: The diversity and co-evolution of RubisCO, plastids, pyrenoids and chloroplast-based CCMs in the algae, *J. Can. Bot.* 76, 1052-1071 (1998)

Balch WM, Holligan, PM, Ackleson, SG, Voss KJ: Biological and optical properties of mesoscale coccolithophore blooms in the Gulf of Maine, *Limnol. Oceanogr.* 36(4), 629-643 (1991)

Billard C: Life cycles, In: Green JC & Leadbeater BS (editors), *The Haptophyte Algae Systematics Association Special Volume* 51, 167-186 (1994)

Bijma J, Spero HJ, Lea DW: Reassessing foraminiferal stable isotope geochemistry: Impact of the oceanic carbonate system (experimental results),. In: *Use of proxies in paleoceanography: Examples from the South Atlantic* (Fischer G & Wefer G, editors), 489–512 (1999)

Bratbak G, Egge JK, Heldal M: Viral mortality of the marine alga *Emilinia huxleyi* (Haptophyceae) and termination of algal blooms, *Mar. Ecol. Progr. Ser.* 93, 39–48 (1993)

Broecker WS, Peng TH: *Tracers in the sea*; Lamont-Doherty Geological Observatory; Columbus University, Palisades, New York (1982)

Buitenhuis ET, Baar HJW, De Veldhuis MJW, Photosynthesis and calcification by *Emiliana huxleyi* (Prymnesiophyceae) as a function of inorganic carbon species, *J. Phycol.* 35(5), 949- 959 (1999)

Davidovich NA, Bates SS: Sexual reproduction in the pinnate diatoms *Pseudonitzschia multiseriata* and *P. pseudodelicatissima* (Bacillariophyceae), *J. Phycol.* 34, 126–137 (1998)

Dickson AG: An exact definition of total alkalinity and a procedure for the estimation of alkalinity and total inorganic carbon from titration data, *Deep-Sea Res.* 28A, 609-623 (1981)

Egge JK, Heimdal BR: Blooms of phytoplankton including *Emiliana huxleyi* (Haptophyta): Effects of nutrient supply in different N:P ratios, *Sarsia* 79, 333-348 (1994)

Elde NC, Morgan G, Winey M, Sperling L, Turkewitz AP: Elucidation of clathrin-mediated endocytosis in *Tetrahymena* reveals an evolutionarily convergent recruitment of dynamin, *PLoS Genetics* 1 e52. DOI: 10.1371/journal.pgen.0010052 (2005)

Elzenga JTM, Prins HBA, Stefels J: The role of extracellular carbonic anhydrase activity in inorganic carbon utilization of *Phaeocystis globosa* (Prymnesiophyceae): A comparison with other marine algae using the isotope disequilibrium technique, *Limnol. Oceanogr.* 45, 372-380 (2000)

Espie, GS, Colman B: Inorganic carbon uptake during photosynthesis: A theoretical analysis using the isotope disequilibrium technique, *Plant Physiol.* 80, 863-869 (1986)

Falkowski PG, Raven JA: *Aquatic Photosynthesis*; Blackwell Publishers (1997)

Falkowski PG, LaRoche J: Acclimation to spectral irradiance in algae, *J. Phycol.* 27(1), 8-14 (1991)

Field MV: Reconstructing the evolution of the endocytic system, in: Jekely G (editor): *Origin and Evolution of Eukaryotic Endomembranes & Cytoskeleton*, Landes Bioscience (2006)

Frada M, Probert I, Allen, MJ, Wilson WH, De Vargas C: The “Cheshire Cat” escape strategy of the coccolithophore *Emiliana huxleyi* in response to viral infection, *PNAS* 105(41) 15944-15949 (2008)

Freeman KH, Hayes JM: Fractionation of carbon isotopes by phytoplankton and estimates of ancient CO₂ levels, *Glob. Biogeochem. Cycles* 6, 185-198 (1992)

Geisen M, Billard C, Broerse ATC, Cros L, Probert I, Young JR: Life cycle associations involving pairs of holococcolithophorid species: Intraspecific variation or cryptic speciation?, *Eur. J. Phycol.* 37, 531–550 (2002)

Gran G: Determinations of the equivalence point in potentiometric titrations of seawater with hydrochloric acid, *Oceanol. Acta* 5, 209-218 (1952)

Green JC: Phagotrophy in prymnesiophyte flagellates, in: Patterson DJ, Larsen J (editors): *The Biology of Free-Living Heterotrophic Flagellates*. The Systematics Association Special Volume 45, 401-414. Oxford: Clarendon Press (1991)

Green JC, Course PA and Tarran GA: The life-cycle of *Emiliana huxleyi*: A brief review and a study of relative ploidy levels using flow cytometry, *J. mar. Syst.* 9, 33-44 (1996)

Guillard RRL, Ryther JH: Studies of marine planktonic diatoms. *Can. J. Microbiol.* 8, 229-239 (1962)

Houdan A, Billard C, Marie D, Not F, Saez AG, Young JR, Probert I: Holococco-lithophore-heterococcolithophore (Haptophyta) lifecycles: flow cytometric analysis of relative ploidy levels, *Systematics and Biodiversity* 1(4), 453–465 (2004)

Houghton JT, Ding Y, Griggs DJ, Noguer M, Van der Linden PJ, Dai X, Maskell K, Johnson CA: *Climate Change 2001: The Scientific Basis: Contribution of Working Group I to the Third Assessment Report of the Intergovernmental Panel of Climate Change* (2001)

Jassby AD, Platt T: Mathematical formulation of the relationship between photosynthesis and light for phytoplankton, *Limnol. Oceanogr.* 21, 540–547 (1976)

John U, Beszteri B, Derelle E, De Peer YV, Read B.: Novel insights into evolution of protistan polyketide synthases through phylogenomic analysis. *Protist* 159, 21–30 (2008)

D. G. Johnson and C. L. Walker, *Annu. Rev. Pharmacol. Toxicol.* 1999. 39:295–312

Johnson KS: Carbon dioxide hydration and dehydration kinetics in seawater, *Limnol. Oceanogr.* 27, 849–855 (1982)

Joint global ocean flux study – Protocols, (1994)

Jones HLJ, Leadbeater BSC, Green JC: Mixotrophy in haptophytes, in: Green JC, Leadbeater BSC (editors): *The Haptophyte Algae*, The Systematics Association Special Volume 51, 209-228, Oxford: Clarendon Press (1994)

Klaas C, Archer DE: Association of sinking organic matter with various types of mineral ballast in the deep sea: Implications for the rain ratio, *Global Biogeochem. Cycles*, 16(4), 1116 (2001)

Klaveness D: *Coccolithus huxleyi* (Lohm.) Kamptn. II. The flagellate cell, aberrant cell types, vegetative propagation and life cycles, *Br. phycol. J.* 7, 309-318 (1972)

Langdon C, Atkinson MJ: Effect of elevated pCO₂ on photosynthesis and calcification of corals and interactions with seasonal change in temperature/irradiance and nutrient enrichment, *J. Geophys. Res.*, 110, C09S07, doi:10.1029/2004JC002576 (2005)

Lewis E, Wallace DWR: Program developed for CO₂ System Calculations. ORNL/CDIAC-105. Carbon Dioxide Information Analysis Center, Oak Ridge National Laboratory, U.S. Department of Energy, Oak Ridge, Tennessee (1997)

Linschooten C, Van Bleijswijk JDL, Van Emburg PR, De Vrind JPM, Kempers ES, Westbroek P, De Vrind-de Jong EW: Role of the light-dark cycle and medium composition on the production of coccoliths by *Emiliana huxleyi* (Haptophyceae), *J. Phycol.* 27(1) 82 – 86 (1991)

Lodish H, Berk A, Kaiser CA, Krieger M, Scott MP, Bretscher A, Ploegh H, Matsuidara P: *Molecular cell biology*, 6th edition, Freeman and company, 847-852 (2008)

MacKinnon SL, Cembella AD, Burton IW, Lewis N, LeBlanc P, Walter JA: Biosynthesis of 13-Desmethyl Spirolide C by the dinoflagellate *Alexandrium ostenfeldii*. *J. Org. Chem.* 71, 8724-8731 (2006)

Marchant HJ, Thomsen HA: Haptophytes in polar waters, in: Green JC, Leadbeater BSC (editors): *The Haptophyte Algae*, The Systematics Association Special Volume 51, 209-228, Oxford: Clarendon Press (1994)

Martin CL, Tortell PD: Bicarbonate transport and extracellular carbonic anhydrase activity in Bering Sea phytoplankton assemblages: Results from isotope disequilibrium experiments, *Limnol. Oceanogr.* 51, 2111–2121 (2006)

McConnaughey T: Acid secretion, calcification and photosynthetic carbon concentrating mechanisms, *Can. J. Bot.* 76, 1119–1126 (1998)

Mook WG, Bommerson JC, Staverman WH: Carbon isotope fractionation between dissolved bicarbonate and gaseous carbon dioxide, *Earth Planet. Sci. Lett.* 22, 169–176 (1974)

Mohan R, Mergulhao LP, Gupta MVS, Rajakumar A, Thamban M, AnilKumar N, Sudhakar M, Ravindra, R: Ecology of Coccolithophores in the Indian sector of the Southern Ocean, *Marine Micropaleontology* 67, 30–45 (2008)

Nielsen MV: Growth, dark respiration and photosynthetic parameters of the coccolithophorid *Emiliana huxleyi* (Prymnesiophyceae) acclimated to different day length – irradiance combinations, *J. Phycol.* 33, 818–822 (1997)

Nimer NA, Merrett MJ: The development of a CO₂-concentrating mechanism in *Emiliana huxleyi*, *New Phytol.* 133, 383-389 (1996)

Nimer NA, Merrett MJ: Calcification and utilization of inorganic carbon by the coccolithophorid *Emiliana huxleyi* Lohmann, *New Phytol.*, 121, 173-177(1992)

Paasche E: A tracer study of the inorganic carbon uptake during coccolith formation and photosynthesis in the coccolithophorid *Coccolithus huxleyi*. *Physiol. Plant. Suppl.* 3, 1-82, 1964

Paasche E: A review of the coccolithophorid *Emiliana huxleyi* (Prymnesiophyceae),

with particular reference to growth, coccolith formation, and calcification-photosynthesis interactions, *Phycologia* 40(6), 503–529, (2002)

Palmqvist K, Yu JW, Badger MR: Carbonic anhydrase activity and inorganic carbonic anhydrase activity in *Chlamydomonas reinhardtii* and *Scenedesmus obliquus*, *Physiol. Plant.* 90, 537-547 (1994)

Rau GH, Riebesell U, Wolf-Gladrow DA: A model of photosynthetic ^{13}C fractionation by marine phytoplankton based on diffusive molecular CO_2 uptake, *Mar. Ecol. Prog. Ser.* 133, 275-285 (1996)

Raven, JA, Johnston, AM: Mechanisms of inorganic-carbon acquisition in marine phytoplankton and their implications for the use of other resources. *Limnol. Oceanogr.* 36: 1701–1714 (1994)

Redfield AC, Ketchum BH, Richards FA: The influence of organisms on the composition of sea-water. In: Hill MN (editor): *The sea, Vol 2. The composition of sea-water comparative and descriptive oceanography.* Interscience Publishers, 26-77 (1963)

Riebesell U and Wolf-Gladrow DA: Supply and uptake of inorganic nutrients, p. 109-140. In P. J. le B. Williams, D. N. Thomas, and C. S. Reynolds [eds.], *Phytoplankton productivity - carbon assimilation in marine and freshwater ecosystems.* Blackwell Science.(2002)

Ridgwell, A. & Zeebe, R. A. 2005. The role of the global carbonate cycle in the regulation and the evolution of the Earth system. *Earth Planet. Sci. Lett.* 234: 299-315.

Riebesell U, Zondervan I, Rost B, Tortell PD, Zeebe RE, Morel FMM: Reduced calcification in marine plankton in response to increased atmospheric CO_2 . *Nature* 407,

634–637 (2000)

Rost B, Zondervan I, Riebesell U: Light-dependent carbon isotope fractionation in the coccolithophorid *Emiliana huxleyi*, *Limnol. Oceanogr.* 47, 120–128 (2002)

Rost B, Riebesell U, Burkhardt S, Sültemeyer D: Carbon acquisition of bloom-forming marine phytoplankton, *Limnol. Oceanogr.* 48, 55–67 (2003)

Rost B, Riebesell U: Coccolithophores and the biological pump: responses to environmental changes, in: *Coccolithophores: from molecular processes to global impact*, Thierstein R, Young JR (editors), Springer, 99–125 (2004)

Rost B, Richter KU, Riebesell U, Hanse PJ: Inorganic carbon acquisition in red tide dinoflagellates. *Plant Cell Environ.* 29, 810–822 (2006)

Rost B, Kranz S, Richter KU, Tortell P: Isotope disequilibrium and mass spectrometric studies of inorganic carbon acquisition by phytoplankton, *Limnol. Oceanogr. Methods* 5, 328–337 (2007)

Saeed AI, Sharov V, White J, Li J, Liang W, Bhagabati N, Braisted J, Klapa M, Currier T, Thiagarajan M: TM4: A free, open source system for microarray data management and analysis, *Biotechniques* 34, 374–378 (2003)

Schlesinger WH: *Biogeochemistry*, Elsevier, 702 (2005)

Sharkey TD, Berry JA: Carbon isotope fractionation of algae as influenced by an inducible CO₂-concentrating mechanism. in: Lucas WJ, Berry J (editors): *Inorganic carbon uptake by aquatic photosynthetic organisms*, *Am. Soc. of Pl. Physiol.*, 389–401 (1985)

Sikes CS, Wheeler AP: Carbonic anhydrase and carbon fixation in coccolithophorids, *J. Phycol* 18, 423-426 (1982)

Sikes CS, Roer RD, Wilbur KM: Photosynthesis and coccolith formation: Inorganic carbon sources and net inorganic reaction of deposition. *Limnol Oceanogr* 25(2), 248–261 (1980)

Silvermann DN: Carbonic anhydrase: Oxygen-18 exchange catalyzed by an enzyme with rate-contributing proton-transfer steps; *Meth. Enzym.* 87, 732-752 (1982)

Staunton J, Weissman, KJ: Polyketide biosynthesis: A millennium review, *Nat. Prod. Rep.* 18, 380-416 (2001)

Stoll MHC, Bakker K, Nobbe GH, Haese RR: Continuous-flow analysis of dissolved inorganic carbon content in seawater. *Anal. Chem.* 73, 4111-4116 (2001)

Storey JD: The positive false discovery rate: A Bayesian interpretation and the Q-Value. Technical of Report 2001-12. Department of Statistics, Stanford University (2001)

Sültemeyer D: Carbonic anhydrase in eukaryotic algae: characterization, regulation, and possible function during photosynthesis. *Can. J. Bot.* 76, 962–72 (1998)

Tillmann U: Kill and eat your predator: a winning strategy of the planktonic flagellate *Prymnesium parvum*, *Aqu. Micr. Ecol.* 32, 73-84 (2003)

Trimborn S, Langer G, Rost B: Effect of varying calcium concentrations and light intensities on calcification and photosynthesis in *Emiliana huxleyi*, *Limnol. Oceanogr.* 52(5), 2285-2293 (2007)

Trimborn S, Lundholm N, Thoms S, Richter KU, Krock B, Hansen PJ, Rost B Inorganic carbon acquisition in potentially toxic and non-toxic diatoms: the effects of pH induced changes in seawater carbonate chemistry. *Physiol Plant*, doi:10.1111/j.1399-3054.2007.01038.x(2008)

Tortell PD, Martin CL, Corkum ME: Inorganic carbon uptake and intracellular assimilation by subarctic Pacific phytoplankton assemblages, *Limnol. Oceanogr.*, 51(5), 2102–2110 (2006)

Tsunogai S., Noriki S. (1991): Particle fluxes of carbonate and organic carbon in the ocean. Is the marine biological activity working as a sink of the atmospheric carbon?; *Tellus*. 43 B: 256-266

Tusher VG, Tibshirani R, Chu G: Significance analysis of microarrays applied to the ionizing radiation response, *Proc. Natl. Acad. Sci.* 98, 5116–5121 (2001)

Volk T, Hoffert MI: Ocean carbon pumps: analysis of relative strengths and efficiencies in ocean-driven atmospheric CO₂ changes, in: *The Carbon Cycle and Atmospheric CO₂: Natural Variations Archean to Present*, Sundquist ET, Broecker WS (edotors), *Geophys Monograph*. 32, 99-110 (1985)

Westbroek P, Young JR, Linschooten K: Coccolith production (Biom mineralization) in the marine alga *Emiliania huxleyi*, *J. Protozool.* 36(4) 368-373 (1989)

Westbroek P, Brown CW, Van Bleijswijk J, Brownlee C, Brummer GJ, Conte M, Egge J, Fernandez E, Jordan R, Knappertsbusch M, Stefels J, Veldhuis M, Van der Wal P, Young JR: A model system approach to biological climate forcing. The example of *Emiliania huxleyi*, *Global Planet. Change* 8, 27–46 (1993)

Winter A, Jordan RW, Roth PH: Biogeography of living coccolithophores in ocean waters, in: Winter A., Siesser WG (editors): Coccolithophores, Cambridge Univ. Press. 1994, 161–177

Wolf-Gladrow DA, Riebesell U, Burkhardt S, Bijma J: Direct effects of CO₂ concentration on growth and isotopic composition of marine plankton, *Tellus* 51(2), 461-476 (1999)

Wright JLC, Cembella AD: Ecophysiology and Biosynthesis of Polyether Marine Biotoxins, in: Anderson DM, Cembella AD, Hallegraeff GM (editors): *Physiological Ecology of Harmful Algal Blooms* 427-451 (1998)

Zondervan I, Zeebe RE, Rost B, Riebesell U: Decreasing marine biogenic calcification: A negative feedback on rising atmospheric pCO₂. *Glob. Biogeochem. Cycles* 15, 507-516 (2001)